Title: Bilateral early activation of retinal microglial cells in a mouse model of unilateral laser-induced experimental ocular hypertension

Rosa de Hoz[1,2#], Ana I. Ramírez[1,2#], Rosa González-Martín[1], Daniel Ajoy[1], Blanca Rojas[1,3], Elena Salobrar-Garcia[1,3], Francisco J. Valiente-Soriano[4], Marcelino Avilés-Trigueros[4], Maria P. Villegas-Pérez[4], Manuel Vidal-Sanz[4], Alberto Triviño[1,3], José M. Ramírez[1,3,*], Juan J. Salazar[1,2,*].

[1]Instituto de Investigaciones Oftalmológicas Ramón Castroviejo. Universidad Complutense de Madrid. Spain.

[2]Facultad de Óptica y Optometría. Departamento de Inmunología, Oftalmología y ORL. Universidad Complutense de Madrid. Spain.

[3]Facultad de Medicina. Departamento de Inmunología, Oftalmología y ORL. Universidad Complutense de Madrid Spain

[4]Departamento de Oftalmología, Facultad de Medicina, Universidad de Murcia and Instituto Murciano de Investigación Biosanitaria Virgen de la Arrixaca. Murcia, Spain

[#]These authors contributed equally to this work

*Corresponding authors:

José M. Ramirez (ramirezs@med.ucm.es), and Juan J. Salazar (jjsalazar@med.ucm.es)

Instituto de Investigaciones Oftalmológicas Ramón Castroviejo.

Facultad de Medicina, Pab 6, 4ª planta. Ciudad Universitaria (UCM).

28040. Madrid. Spain.

e-mail address:

Rosa de Hoz: rdehoz@med.ucm.es;
Ana I. Ramírez: airamirez@med.ucm.es,
Rosa González-Martín: rosagonz@ucm.es,
Daniel Ajoy: dajoym@gmail.com,
Blanca Rojas: brojas@med.ucm.es,
Elena Salobrar-García: elenasalobrar@med.ucm.es,
Francisco J. Valiente: fjvaliente@um.es,
Marcelino Avilés-Trigueros: marcelin@um.es,
Maria P. Villegas-Pérez: mpville@um.es,
Manuel Vidal-Sanz: manuel.vidal@um.es,
Alberto Triviño: atrivino@med.ucm.es,

Abstract

The immune system plays an important role in glaucomatous neurodegeneration. Retinal microglial reactivation associated with ganglion cell loss could reportedly contribute to the glaucoma progression. Recently we have described signs of microglia activation both in contralateral and ocular hypertension (OHT) eyes involving all retinal layers 15 days after OHT laser induction in mice. However, no works available have analyzed the microglial activation at earliest time points after OHT induction (24h) in this experimental model. Thus, we seek to describe and quantify signs of microglia activation and differences depending on the retinal layer, 24 h after unilateral laser-induced OHT. Two groups of adult Swiss mice were used: age-matched control (naïve) and lasered. In the lasered animals, OHT eyes as well as contralateral eyes were analyzed. Retinal whole-mounts were immunostained with antibodies against Iba-1 and MHC-II. We quantified the number of microglial cells in the photoreceptor layer (OS), outer plexiform layer (OPL), and inner plexiform layer (IPL); the number of microglial vertical processes connecting the OPL and OS; the area of the retina occupied by Iba-1+ cells (Iba1-RA) in the nerve fiber layer-ganglion cell layer (NFL-GCL), the total arbor area of microglial cells in the OPL and IPL and; Iba-1+ cell body area in the OPL, IPL and NFL-GCL. In contralateral and OHT eyes the morphological features of Iba-1+ cell activation were: migration, enlargement of the cell body, higher degree of branching and reorientation of the processes, radial disposition of the soma and processes toward adjacent microglial plexuses, and presence of amoeboid cells acting as macrophages. These signs were more pronounced in OHT eyes. Most of Iba-1+ cells did not express MHC-II; rather, only dendritic and rounded cells expressed it. In comparison with naïve eyes, in OHT eyes and contralateral eyes

no significant differences were found in the microglial cell number; but there was a significant increase in Iba1-RA. The total arbor area of microglial cells was significantly decreased in: i) OHT eyes with respect contralateral eyes and naïve-eyes in IPL; ii) OHT eyes with respect to naïve eyes in OPL. The number of microglial vertical processes connecting the OPL and OS were significantly increased in contralateral eyes compared with naïve-eyes and OHT eyes. In OPL, IPL and NFL-GCL, the cell body area of Iba-1+ cells was significantly greater in OHT eyes than in naïve and contralateral eyes, and greater in contralateral eyes than in naïve eyes. A non-proliferative microglial reactivation was detected both in contralateral eyes and in OHT eyes in an early time after unilateral laser-induced OHT (24 hours). This fast microglial activation, which involves the contralateral eye, could be mediated by the immune system.

Highlights

- 24h after laser-induced OHT, a non-proliferative microglial reactivation was shown both in OHT eyes and their contralateral untreated eyes.
- This fast microglial activation in both eyes could be mediated by the immune system.

Keywords: microglia; retina; contralateral; early activation; ocular hypertension; experimental glaucoma; MHC-II; Iba-1.

Abbreviations:

GCL (ganglion cell layer)

IOP (intraocular pressure)

IPL (inner plexiform layer)

Iba1-RA (area of the retina occupied by Iba-1+ cells)

MHC-II (major histocompatibility complex class II)

NFL (nerve fiber layer)

OHT (ocular hypertension)

OS (photoreceptor layer)

OPL (outer plexiform layer)

RGC (retinal ganglion cell)

Funding: This work was supported by: i) the Ophthalmological Network OFTARED (RD16/0008/0005, RD16/0008/0026 , of the Institute of Health of Carlos III of the Spanish Ministry of Economy; by the PN I+D+i 2008–2011, by the ISCIII-Subdirección General de Redes y Centros de Investigación Cooperativa, and by the European programme FEDER; ii) SAF-2014-53779-R and SAF2015-67643-P from the Spanish Ministry of Economy and Competitiveness and; iii) Fundación Séneca, Agencia de Ciencia y Tecnología Región de Murcia (19881/GERM/15). Grants to Elena Salobrar-Garcia are currently supported by a Predoctoral Fellowship (FPU13/01910) from the Spanish Ministry of Education, Culture and Sport.

1. Introduction

Glaucoma is a neurodegenerative disease characterized by retinal ganglion cell (RGC) loss. Classically, intraocular pressure (IOP) has been considered the main glaucoma risk factor treatable at present (Quigley and Broman, 2006). However, IOP control does not always delay the progression of the disease.

It has been demonstrated that in glaucomatous neurodegeneration the immune system plays an important role (Tezel and the Fourth ARVO/Pfizer Ophthalmics Research Institute Conference, Working Group, 2009). In the central nervous system, the microglia is the principal immunocompetent cell (Bosco et al., 2011; Streit et al., 2005). This cell responds to neuronal damage by adopting an activated phenotype (de Hoz et al., 2013; Gallego et al., 2012; Rojas et al., 2014), which is characterized by morphological changes (retraction, reorientation and hyper-ramification of the processes and presence of different morphological types such as hyper-ramified, rod-like, and amoeboid microglia), migration, proliferation, and accumulation around the injured areas. In addition, activated microglia can alter the expression of receptors (CX3CR1, P2Y12 and CD200R1) and enzymes (metalloproteinases, collagenases and furin) and secrete cytotoxic substances such as proinflammatory cytokines, proteases, and oxygen-free radicals. In addition, these activated cells can act as antigen-presenting cells, and can transform into phagocytes (Karlstetter et al., 2015; Karlstetter et al., 2015; Kettenmann et al., 2011; Kettenmann et al., 2011; Luo et al., 2010; Luo et al., 2010; Ramírez et al., 2015; Ransohoff and Perry, 2009). Microglial reactivation has been associated with RGC loss in human glaucoma (Yuan and Neufeld, 2001) and in experimental models of glaucoma (de Hoz et al., 2013; Gallego et al., 2012; Rojas et al., 2014), which could contribute to the glaucoma progression (Madeira et al., 2015). The inhibition of microglial activation by minocycline

(Bosco et al., 2008) or with a high dose of irradiation (Bosco et al., 2012) can decrease RGC death.

In our previous studies in a mouse model of unilateral laser-induced ocular hypertension (OHT), we demonstrated that, 15 days after laser treatment, microglia showed several quantitative and qualitative signs of activation. These signs mainly included: i) shortening and widening of microglial processes (consistent with the significant reduction of the microglia arbor area); the presence of a high degree of branching (hyper-ramified microglia); microglial migration across the retinal parenchyma; increased microglial number; presence of CD68 amoeboid microglia acting as macrophages; presence of rod-like microglia (only in OHT eyes) which could be related with the synaptic stripping (a process in which microglia selectively remove synapses from injured neurons) (Blinzinger and Kreutzberg, 1968; Trapp et al., 2007); and MHC-II up-regulation in cells of all retinal layers. These microglial activation signs were detected in the OHT eye but also in the untreated contralateral normotensive eye. The microglial activation in the contralateral eye 15 days after laser treatment could reflect the initial events of OHT-induced neurodegeneration, probably mediated by inflammatory mechanisms (de Hoz et al., 2013; Gallego et al., 2012; Rojas et al., 2014). However, it is unknown whether microglial activation is an early process occurring after laser induced IOP elevation through photocoagulation of the limbal and episcleral veins, not only in OHT eye but also in the normotensive contralateral eye. If this activation occurs early after the induction of the OHT (24 h), it could be informative to analyze the specific characteristics of retinal microglial activation in both OHT and contralateral normotensive eyes.

Few studies examine early retinal microglial activation (2 h to 4 days) after OHT induction in experimental models (Wang et al., 2000; Naskar et al., 2002; Zhang et al., 2005; Fu and Sretavan, 2010; Wang et al., 2014; Ha et al., 2015; Trost et al., 2015), and even more, those who use the mouse for that purpose (Fu and Sretavan, 2010; Naskar et al., 2002; Wang et al., 2000). Only three studies (Bodeutsch et al., 1999; Wang et al., 2000; Zhang et al., 2005) analyze microglial activation at 24 h after retinal injury, and these have been performed in rats. Two of these studies, use models to induce OHT different from ours, such as the acute elevation of intraocular pressure (raised to 120 mmHg for 60 min by saline injection in the anterior chamber) (Zhang et al., 2005) and the episcleral vein cauterization (Wang et al., 2000). The third uses another mechanism to inflict retinal damage, the optic-nerve crush (Bodeutsch et al., 1999). Thus, no available studies using the OHT mouse model of the present study analyze the early (24 h) changes in retinal microglia. Nevertheless, none describes in detail the microglial activation in the damaged eye and in its contralateral undamaged eye.

Thus, the aim of the present study was to analyze in retinal whole-mounts, at an early time after laser- induced OHT (24 h), the distinctive signs of microglial activation in the different retinal layers, both in OHT eyes and in contralateral eyes, including: microglia cell number, cell arbor area in the plexiform layers, area occupied by Iba-1+ cells (Iba 1-RA) in the NFL-GCL, number of microglial vertical processes connecting the OPL and OS, MHC-II- upregulation, and cell body area of Iba-1+ cells in the OPL,IPL and NFL- GCL, -.

2. Materials and methods

2.1. Ethics statement

Mice were treated in accordance with Spanish law and the Guidelines for Humane Endpoints for Animals Used in Biomedical Research. This study was approved by the Ethics Committee for Animal Research of Murcia University (Murcia, Spain) and the Animal Health Service of the Murcia Regional Ministry of Agriculture and Water (approval ID number: A1310110807). In addition, animal procedures followed institutional guidelines, European Union regulations for the use of animals in research, and the Association for Research in Vision and Ophthalmology (ARVO) statement for the use of animals in ophthalmic and vision research.

2.2. Animals and anesthetics

The experiments were performed on adult male albino Swiss mice (between 40 and 45g) obtained from the breeding colony of the University of Murcia. The animals were housed in temperature- and light-controlled rooms with a 12 h light/dark cycle and *ad libitum* access to food and water. Light intensity within the cages ranged from 9 to 24 lux. Surgical procedures, including IOP measurement, were performed under general anesthesia induced with an intraperitoneal (ip) injection of a mixture of ketamine (75 mg/kg, Ketolar®, Parke-Davies, Barcelona, Spain) and xylazine (10 mg/kg, Rompún®, Bayer, Barcelona, Spain). During recovery from anesthesia, the mice were placed in their cages and an ointment containing tobramycin (Tobrex®; Alcon, Barcelona, Spain) was applied to the cornea to prevent corneal desiccation and infection. Additional measures were taken to minimize discomfort and pain after surgery. The animals were killed with an ip overdose of pentobarbital (Dolethal Vetoquinol®, Especialidades Veterinarias, Alcobendas, Madrid, Spain).

2.3. Experimental groups

Two groups of mice were considered for study: an age-matched control (naïve, n=6) and a lasered group (n=6) this last group was processed 24 h after lasering.

2.4. Laser treatment and Intraocular pressure (IOP) measurements

To induce OHT, the left eyes of anesthetized mice were treated in a single session with a series of diode laser burns (Viridis Ophthalmic Photocoagulator-532 nm, Quantel Medical, Clermont-Ferrand, France) following previously described methods (Cuenca et al., 2010; Salinas-Navarro et al., 2009). In brief, the laser beam was directly delivered without any lenses, aimed at the limbal and episcleral veins. The spot size, duration, and power were between 50 to 100 μm, 0.5 seconds and 0.3 W, respectively. Each eye received between 55 to 76 burns. The IOP of the six mice in which OHT was induced was measured under deep anesthesia in both eyes (treated eye as well as the contralateral intact fellow eye) with a rebound tonometer (Tono-Lab, Tiolat, OY, Helsinki, Finland) (Naskar et al., 2002; Quigley and Hohman, 1983) prior to laser induction, and 24 h after laser treatment for the lasered group and before the animals were killed for the naïve. To avoid fluctuations of the IOP due to the circadian rhythm in albino Swiss mice (Neufeld, 1999) or due to the increase in the IOP itself (Yuan and Neufeld, 2001), we tested the IOP consistently around the same time, preferentially at 9 a.m. and directly after deep anesthesia in all animals (lasered group and naïve). Six consecutive readings were made for each eye and averaged.

2.5. Immunohistochemistry

The mice were deeply anesthetized as mentioned above, perfused transcardially through the ascending aorta first with saline and then with 4% paraformaldehyde in 0.1 M phosphate buffer (PB) (pH 7.4). The orientation of each eye was carefully

maintained with a suture placed on the superior pole immediately after deep anesthesia and before perfusion fixation. Moreover, upon dissection of the eye, the insertion of the rectus muscle and the nasal caruncle were used as additional landmarks (Shimazawa et al., 2005). The eyes were post-fixed for two hours in the same fixative and kept in sterile 0.1 M PB. The retinas were then dissected, vitreous humor was removed using atraumatic clamps and Westcott scissors (vitrectomy), and finally the retinas were processed as retinal whole-mounts (Levkovitch-Verbin et al., 2006; Triviño et al., 1992).

For the analysis of the microglial population in the mice retina and the expression of MHC class II molecules, retinal whole-mounts were immunostained, as described elsewhere (Gallego et al., 2012). The following primary antibodies were used: rabbit anti-Iba-1 (Wako, Osaka, Japan) in a 1:600 dilution and rat anti-mouse MHC class II (I-A/I-E) (eBioscience; San Diego, CA, USA) in a 1:100 dilution. The solution used to dilute primary antibodies was made up by 1% animal serum in which the corresponding secondary antibody was developed plus 0.1% triton-X in phosphate-buffered saline (PBS). Binding sites of the primary antibodies were visualized with the corresponding secondary antibodies: donkey anti-rabbit Alexa Fluor 594 (Invitrogen, Paisley, United Kingdom) in a 1:800 dilution and donkey anti-rat Alexa Fluor 488 (Invitrogen, Paisley, United Kingdom) in a 1:150 dilution. Secondary antibodies were diluted in PBS.

In all instances, a negative control was performed to demonstrate that the secondary antibody reacted only with its respective primary antibody. This control was made by eliminating the primary antibody and replacing it with the solution used to dilute primary antibodies, which should result in the absence of immunoreactivity. In addition to identifying the contribution of the endogenous

fluorescence to the observed label, a tissue sample was incubated in all the buffers and detergents used in the experiment but without antibodies (Triviño et al., 2002).

Retinas were analyzed and photographed with the ApoTome device (Carl Zeiss, Munich, Germany) and with a digital high-resolution camera (Cool- SNAP Photometrics, Tucson, AZ, USA) coupled to a fluorescence microscope (Axioplan 2 Imaging Microscope Carl Zeiss, Munich, Germany). The microscope was equipped with appropriate filters for fluorescence-emission spectra of Alexa fluor 488 (Filter set 10, Zeiss) and Alexa fluor 594 (Filter set 64, Zeiss). The ApoTome uses the 'structured illumination' method that enables conventional microscopy to create optical sections through the specimen and thereby improve the contrast and resolution along the optical axis. Each retinal whole-mount was analyzed using the motorized stage of the microscope to scan the entire preparation along the x, y and z axes. Cellular components in the same xz plane were considered to lie in the same focal plane. Z-stacks acquired were analyzed in Axiovision version 4.2 (Carl Zeiss, Munich, Germany) with Inside4D (3D View) tool in order to perform cut-view analysis. A cut-view is a software-generated reconstruction of the xz and yz planes of the z-stack, allowing visualization through the depth of the acquired z-stack.

Adobe Photoshop CS3 Extended 10.0 (Adobe Systems, Inc., San Jose, California, USA) was used for figure preparation.

2.6. Quantitative Retinal analysis

To determine the effect of OHT on Iba-1+ cells 24 h after lasering, we quantified: the number of microglial cells in the outer segment layer (OS), outer plexiform layer (OPL) and inner plexiform layer (IPL); the area of the retina occupied by

Iba-1+ cells (Iba1-RA) in the NFL-GCL, the arbor area of the Iba-1+ cells in the OPL and IPL, the number of microglial vertical processes connecting the OPL and OS, and the cell body area of Iba-1+ cells in the OPL, IPL and NFL-GCL. The OS, OPL, IPL, and NFL-GCL were identified by the different morphologies exhibited by the microglia in each retinal layer. In addition, the transition from one retinal layer to another was recognized by the weak autofluorescence emitted by the somas of the nuclear layers with the filter for fluorescence-emission spectra of 488 nm (green). The quantifications were performed in the retinal whole-mounts of naïve (n = 6), contralateral (n = 6), and OHT eyes (n = 6) following methods previously described by us (Gallego and de Gracia, 2016; Rojas et al., 2014). In brief, equivalent areas of the retina were selected for each retinal whole-mount, both in the vertical and in the horizontal meridians (Fig. 1A). These areas were photographed at 20x, giving an area of 0.1502 mm^2 per field, and analyzed along the X-Y axis. The quantification method used depended on the cell number and cell-distribution characteristics of each retinal layer. In the IPL and OPL, Iba-1+ cells formed a cellular network (they were distributed throughout the retina in a mosaic-like fashion) without overlap between them, allowing their individual identification, thus meeting the criteria for automatic cell counting (Fig. 1B). By contrast, in the NFL-GCL the distribution of Iba-1+ cells makes it difficult to distinguish one from another, preventing the use of automatic cell counting. As a result of this limitation, we quantified the area of the retina occupied by Iba-1+ cells (Iba1-RA) in this retinal layer (Fig. 1C). In the OS, Iba-1+ cells were counted manually because they did not form a regular plexus (one of the algorithm criteria for automatic counting being applied) and individual cells could be differentiated from each other.

2.6.1. Number of microglial cells in the OS

For this quantification, we used the Interactive measurement, a manual counting tool included in the AxioVision Release 4.8.2 computer program (Zeiss, Germany) in association with the ApoTome device coupled to the fluorescence microscope.

2.6.2. Quantification of microglial cells in the OPL, IPL and the NFL-GCL

For this, we used a new quick and reliable algorithm of segmentation and control of distances developed in MATLAB for automatic microglial cell quantification, created by our group (Fig. 1B). This algorithm enabled the quantification of microglial cell number in the OPL and IPL and evaluated the Iba1-RA. Briefly, the algorithm we use for iba1+cell counting consists of: first, averaging the Z-stack of images selected (Fig. 1B1). The result of this operation is referred to as the Z projection (Fig. 1B2); afterwards, in the Z-projection image, we performed two different operations in order to preserve only the most intense part of microglial cells, these usually being the somas, which we will use to identify and quantify them. In the first operation, the image is normalized to the pixel with the maximum value in the image, after which the image values are within a range from 0 to 1. We do this because, by thresholding, the second operation sets all the values under 0.2 and preserves the rest (Fig. 1B3). Afterwards, we segment the resulting image (Fig. 1B4) and calculate the center of mass of each of these segments to identify the presence or absence of cells in all cases (Fig. 1B5). In the event that 2 or more adjacent segments have positive signal from the same cell, the algorithm count each segment as different events. Therefore, to discard these false positives, we introduced a condition of minimum distance between 2 different cells (Fig. 1B6 inset). All points that were within that minimum distance

were considered to belong to the same cell and only one of the points was counted as a cell. After all of these operations the algorithm gives us the final results of automatic microglial-cell counting in the OPL and IPL (Fig. 1B6). (de Gracia et al., 2015; Gallego and de Gracia, 2016).

As mentioned above, the NFL-GCL did not fulfill the criteria for automatic individual cell counting with MATLAB, and therefore we quantified the area of the retina occupied by Iba-1+ cells (Iba1-RA) in each photograph selected. For this images of the NFL-GCL were processed with a threshold tool in MATLABb (Fig. 1C). Thresholding defines a range of gray-scale values found on the pixels of objects of interest, differentiating them from other parts of the image based on the image's gray scale. The threshold tool in MATLAB enabled us to change the values for the threshold of the NFL to evaluate the retinal area immunolabeled with Iba-1. Afterwards, when the pixel value information is used, the button "Count NFL" evaluates the percentage of image immunolabeled in a single selected image (Gallego and de Gracia, 2016).

2.6.3. Arbor area of the Iba-1+ cells in the OPL and the IPL

Among the areas selected for microglia quantification, along the vertical and horizontal meridian that crosses the optic nerve, we consistently analyzed 4 equivalent areas in each plexiform layer. For consistent results, the retinal areas selected were located at specific distances from the optic disc in the different quadrants of the retina. Thus, in the superior retinas, we selected the retinal area closest to the optic disc and in the inferior, nasal, and temporal retinas the areas analyzed were located at two, three or four levels of eccentricity from the optic disc, respectively. In the 20x microphotographs selected by this method, the arbor area of Iba-1+ cells in the plexiform layers was quantified with a computer-

assisted morphometric analysis method previously described (Rojas et al., 2014). A polygon was drawn manually by connecting the distal-most tips of the Iba-1+ cell processes using the Interactive Measurement, tool of AxioVision (Zeiss, Germany), in association with the ApoTome device coupled to the fluorescence microscope.

2.6.4. Number of microglial vertical processes connecting the OPL and OS

In the four retinal areas selected for arbor area quantification, photographs were made at 20x in the plane between OPL and OS. The Iba-1+ spots, which corresponded to the optical transversal sections of the vertical processes of Iba-1+ microglial cells that connect the OPL and OS, were quantified using the manual counting tool included in the AxioVision mentioned above.

2.6.5. Cell body area of Iba-1+ cells in the OPL, IPL and NFL-GCL

Microphotographs (20x) were taken in the OPL, IPL and NFL-GCL layers in the same four retinal areas used for quantification of arbor area. The contour of cell bodies of Iba-1+ cells were traced manually, and cell body area was determined using the "interactive measurement tool" in AxioVision software (Zeiss, Germany).

2.7. Statistical analysis

Data for the statistical analysis were introduced and processed in a SPSS 22 (comprehensive statistical software; SPSS Inc©, Armonk, New York, USA). Data are shown as mean ± SD. Statistical analyses were performed with Mann Whitney U test (Unpaired data) or Wilcoxon W test (paired data) to identify differences among of the OHT, contralateral and naïve eyes as follows: i) IOP values; ii) Iba-1+ cell number in the OS, OPL and IPL; iii) Iba1-RA in the NFL-GCL; iv) arbor area of the Iba-1+ cells in the OPL and IPL v) number of microglial

vertical processes connecting the OPL and OS and; vi) cell body area of Iba-1+ cells in the OPL, IPL and NFL-GCL. Differences were considered significant when P <0.05.

3. Results

3.1. Laser-induced ocular hypertension

The IOP values of OHT eyes 24 h after laser induction (35.57 ± 7.4 mmHg) significantly differed from naïve values (15.80 ± 2.12 mmHg) ($p<0.001$ with Mann Whitney U test) and contralateral values (15.02 ± 0.42) ($p<0.05$ with Wilcoxon W test). No significant differences were found between contralateral and naïve values.

3.2. General distribution of Iba-1+ cells throughout retinal extension

At low magnification (5x and 10x), in naïve and contralateral eyes Iba-1+ cells were evenly distributed throughout the retina from the optic disc to the periphery (Fig. 2A). However, in the OHT group the distribution of Iba-1+ cells was not homogeneous (Fig. 2B); specifically, in their retinal periphery, there were areas of Iba-1+ cell scarcity, in which the cells even disappeared (Fig. 2B,C). In all the OHT eyes analyzed, these areas were large and located mainly in the peripheral superior zone of the retina (Fig. 2B). In addition, smaller areas of Iba-1+ cell scarcity were also observed in the periphery of the temporal, inferior and nasal zones of the retina (Fig. 2B). However, these smaller zones were not found in all OHT retinas analyzed.

3.3. Morphology and distribution of Iba-1+ cells in the different retinal layers

405 In all study groups, the Iba-1+ cells were distributed in different retinal layers:
406 NFL-GCL, IPL, OPL, and OS. In naïve retinas, the general characteristics of the
407 Iba-1+ cells specific to each layer have been previously described by our group
408 (Rojas et al., 2014).

409 **3.3.1. Iba-1+ cells in the NFL-GCL**

410 In naïve eyes, two morphological types of Iba-1+ cells have been described
411 (Rojas et al., 2014), i.e. ramified and perivascular. In comparison with naïve (Fig.
412 3A,B) both cell types in contralateral and in OHT eyes showed : i) a retraction of
413 the cell processes (Fig. 3C-F), ii) enlargement of the cell body (Fig. 3C-F, Fig. 14)
414 and, iii) some cells that arranged radially sending processes to the IPL plexus.
415 These findings were more pronounced in OHT eyes (Fig. 3E,F; Fig. 4C, Fig. 14).
416 In OHT eyes (Fig. 2B,C, Fig. 6A-D) the plexus formed by the ramified Iba-1+ cells
417 were disrupted at the border of the areas of Iba-1+ cell scarcity.

418 Additional morphological types of Iba-1+ cells were found in the contralateral and
419 OHT retinas, these including: cells with an amoeboid morphology (Fig. 4B,D,E;
420 Fig. 6G) and rounded cells (Fig. 5A,C, Fig. 6A,C,E). These cell types were found
421 more frequently near to the optic disc (Fig. 6E) and in the retinal periphery close
422 to the areas of Iba-1+ cell scarcity (Fig. 6A,C), but were scant in contralateral
423 eyes. Rounded Iba-1+ cells were in close relation with ramified Iba-1+ cells, which
424 seemed to catch the rounded cells with their processes (Fig. 5A,C). In OHT eyes,
425 some amoeboid Iba-1+ cells had vacuoles inside (Fig. 4D, Fig. 6G) and showed
426 small vesicles both in the surface of the cell body and in their vicinity (Fig. 4D).

427 Other morphological Iba-1+ cell types were observed occasionally in some OHT
428 eyes: i) rod-like cells (cells with elongated bodies and processes that prominently

429 project from the basal and apical ends), two or three per retina (Fig. 4F); ii)
430 ramified cells from the IPL, which could have migrated to the NFL-GCL (Fig. 4G);
431 and iii) dendritic-like cells (Fig. 4H).

432 **3.3.2. Iba-1+ cells in the IPL**

433 In naïve eyes two morphological types of Iba-1+ cells have been described, i.e.
434 ramified and dendritic-like cells (Rojas et al., 2014).

435 In contralateral and OHT eyes (Fig. 7B-E) in comparison to naïve eyes (Fig. 7A),
436 ramified Iba-1+ cells exhibited: i) a disappearance of their distribution in a
437 mosaic–like fashion (without overlapping between neighboring cells) throughout
438 the retina, which was caused by the approach or separation among microglial
439 cells in some retinal zones (Fig. 7B,C). In OHT eyes, some cell processes were
440 so close together that it was difficult to discern a space between them (Fig. 7C);
441 ii) enlargement of the cell body (Fig. 7B-E, Fig. 14); and iii) an increase in the
442 secondary and superior order processes (Fig. 7B-D). Ramified Iba-1+ cells
443 changes were more pronounced in OHT eyes (Fig. 7C-E) than in contralateral
444 eyes (Fig. 7B). In addition, in OHT eyes, there was a retraction of the cell
445 processes (Fig. 7C-E) and some ramified cells migrate to the NFL-GCL (Fig. 4G).
446 In the areas of Iba-1+ cell scarcity, the ramified Iba-1+ cells were not detected,
447 and ramified Iba-1+ cells near those areas reoriented their processes toward
448 them (Fig. 7D). Some of these cells became thicker and lost fine processes,
449 which showed spheroidal swelling (Fig. 7E).

450 In naïve eyes, dendritic-like cells ran parallel to the retinal surface and were
451 located in the juxtapapillary area and near the collecting tube venule in the
452 peripheral retina (Rojas et al., 2014). These cells were more frequently detected

453 in contralateral and OHT eyes than in naïve (Fig. 7 F-H) and could even form
454 rows of cells parallel to the vascular pathway.

455 **3.3.3. Iba-1+ cells in the OPL**

456 In the OPL of naïve, contralateral, and OHT eyes, only ramified Iba-1+ cells have
457 been described (Rojas et al., 2014). In comparison with naïve eyes (Fig. 8A),
458 ramified Iba-1+ cells in contralateral and OHT eyes exhibited: i) enlargement of
459 the cell body, which was more evident in OHT eyes than in contralateral eyes
460 (Fig. 8B-C, Fig. 14); ii) numerous thin and short secondary and superior order
461 processes (Fig. 8B-C); iii) greater number of processes reaching the OS (Fig. 8E,
462 Fig. 9A,B). This characteristic was more pronounced in contralateral eyes, in
463 which Iba-1+ cells of OPL projected several long processes that reached the OS
464 (Fig. 8E, 9A,B, 10K). In this latter layer, processes from the OPL branched
465 profusely (Fig. 10J,K) and became located near to Iba-1+ cells of OS (Fig. 8E);
466 and iv) the network of Iba-1+ cells without overlapping between neighboring cells
467 throughout the retina observed in naïve eyes (Fig. 8A) (mosaic-like fashion
468 distribution) was disrupted in some areas of the OPL (Fig. 8C) for two reasons.
469 The first was the presence of smaller cells (Fig. 8C,D), which, after being
470 analyzed in the cut-view in the yz (sagittal) tool of the microscope, corresponded
471 to ramified Iba-1+ cells which changed their arrangement of being parallel to
472 being perpendicular to the retinal surface (radial cells) (Fig. 8D,G,H). Radial cells
473 were found more frequently in OHT eyes (Fig. 8H). The second reason was the
474 approach of the processes of ramified cells toward radial cells surrounding them
475 (Fig. 8C,D). The processes of microglial cells in the OPL were so close together
476 that there was sometimes only a small cleft between them (Fig. 8F).

On the other hand, in the OHT eyes the ramified Iba- 1+ cells had disappeared in the areas of Iba-1+ cell scarcity and the Iba-1+ cells next to this area reoriented their processes toward it (Fig. 8G). In the areas of Iba-1+ cell scarcity, Iba-1+ cells with apparently amoeboid morphology were sometimes seen (Fig. 8G). However, after they were analyzed in the cut-view in the yz (sagittal) tool of the microscope, these cells were found not to be amoeboid cells, but rather had a radial disposition, had a great retraction of their processes, and were located between OPL and OS (Fig. 8 G,H).

3.3.4. Iba-1+ cells in the OS

In naïve eyes, two morphological types of Iba-1+ cells have been described in the OS, depending on their morphology and location: i) Type 1- OS cells with ovoid somas located near or inside the ONL, and numerous processes which emerged from the same point of the soma, like the roots of a tree. This cell type was arranged perpendicular to the retinal surface (Fig. 10A,B); and ii) Type 2- OS cells with ovoid somas located near the retinal pigment epithelium (RPE) and one thick primary process running parallel to the retinal surface. Sparse, thin, and short processes sprout from the soma and the primary process (Fig. 10C). Both Iba-1+ OS cell types are unevenly distributed in the OS (Rojas et al., 2014).

As in naïve eyes, both in contralateral eyes and OHT eyes, Iba-1+ cells were not evenly distributed, grouping in some areas and leaving others empty. Overall, no Iba-1+ cells were detected in the areas of Iba-1+ cell scarcity in OHT eyes except some amoeboid Iba-1+ cells that grouped in clusters.

In OHT eyes and contralateral eyes, Type 1-OS and Type 2-OS cells showed changes in their morphology and arrangement: i) most Type 1-OS Iba-1+ cells

changed the orientation of their processes from perpendicular to parallel to the retinal surface (Fig. 10D,E,L). This cell type was the one most frequently observed in contralateral eyes. A thick process occasionally emerged from the radial Type 1-OS cells and reached the OPL plexus (Fig. 10F) and; ii) Type 2-OS cells had numerous thin processes sprouting from the soma and the thick process giving them a "hairy" appearance as previously described (Rojas et al., 2014) (Fig. 10G,M).

Additional morphological cell types were found in the OS in OHT and contralateral eyes: Both were more frequently observed in the former i) amoeboid Iba-1+ cells, which were the predominant cell type in the OHT eyes (Fig. 10H,L) and; ii) dystrophic microglia (Fig. 10 I,N). Streit et al. defined dystrophic microglia as those cells "displaying abnormal morphological features, such as shortened, gnarled, beaded, or fragmented cytoplasmic processes, as well as loss of fine ramifications and formation of spheroidal swellings" (Streit et al., 2014).

3.3.5. Iba-1+ cells between IPL-OPL-OS

Some Iba-1+ cells from IPL or OPL changed their arrangement of being parallel to the retinal surface to a radial disposition (Fig. 9A, Fig. 9C, Fig. 10O) and their somas were localized in the INL or in the ONL. The processes of these radial Iba-1+ cells could participate in the microglial plexuses of the IPL and the OPL. This feature was more frequently observed in OHT eyes. However, in the contralateral eyes microglial cells of IPL (Fig. 9B), OPL (Fig. 8E, Fig. 9A,B, Fig. 10K), and OS (Fig. 10F) sent numerous processes to the nearest retinal layers (from IPL to NFL-GCL and OPL, from OPL to IPL and OS and from OS to OPL), thus forming part of the neighboring microglial plexuses. The processes and somas of the

radial cells could contribute, as mentioned above, to the alteration of the pattern of the microglial mosaic in some areas of the OPL and IPL.

3.3.6. MHC-II expression

In OHT and contralateral eyes, MHC-II expression was mostly restricted to the dendritic-like cells (Fig. 4H,I, Fig. 7G,H,J,K), as in naïve eyes (Fig. 7F,I), and to some of the rounded cells (Fig. 5, Fig. 6A-F). In OHT eyes numerous rounded MHC-II+ cells were observed in the vicinity of the optic disc (Fig. 6E,F), along with some of the large retinal vessels and in the areas of Iba-1+ cell scarcity, mainly in the superior zone (Fig. 6A-D). These cells exhibited an intense MHC-II immunostaining and yet their Iba-1 expression was variable, finding strong Iba-1+ immunostaining and Iba-1 negative immunostaining cells. Rounded MHC-II+ cells, though abundant in NFL-CGL, were also found in the OS but rarely in the OPL. Overall, rounded MHC-II+ cells were in close relation with ramified and amoeboid Iba-1+ cells. This fact was remarkable in the NFL-CGL layer were many ramified Iba-1+ cells grasped rounded MHC-II+ cells (Fig. 5A-D). Amoeboid cells, chiefly in the GCL-NFL, approached the rounded MHC-II+ cells. Some of these amoeboid cells had MHC-II+ vacuoles inside (Fig. 6G, H). In addition, some of the scarce rod-like Iba-1+ cells observed exhibited MHC-II expression.

In contralateral eyes very scarce rounded cells exhibited a MHC-II expression (Fig. 5 A,B).

3.4. Quantitative analysis of Iba-1 retinal microglial cells

3.4.1. Number of Iba-1+ cells in the IPL, OPL, and OS

No significant differences were found in the microglial cell number of IPL, OPL and OS between naïve, OHT eyes and contralateral eyes (Mann Whitney U test) (Table 1).

3.4.2. Area of the retina occupied by Iba-1+ cells (Iba1-RA) in NFL-GCL

In the NFL-GCL, the Iba1-RA significantly increased in both contralateral and in OHT eyes compared to naïve ($p<0.01$ in both instances, Mann Whitney U test). In OHT eyes the Iba1-RA was significantly higher than in contralateral eyes ($p<0.05$, Wilcoxon W test) (Fig. 11).

3.4.3. Quantification of the arbor area of the Iba-1+ cells

In the OPL, the arbor area of the Iba-1+ cells significantly decreased in OHT eyes with respect to naïve eyes ($p<0.05$, Mann Whitney U test). No significant differences were found between OHT eyes and contralateral eyes, and in contralateral eyes with respect to naïve eyes (Fig. 12).

In the IPL the arbor area of the Iba-1+ cells significantly decreased in OHT eyes with respect naïve eyes and contralateral eyes ($p<0.01$, Mann Whitney U test and $p<0.05$, Wilcoxon W test, respectively). No significant differences were found in contralateral eyes with respect to naïve eyes (Fig. 12).

3.4.4 Quantification of microglial vertical process

In contralateral untreated eyes, the number of microglial vertical processes connecting the OPL and OS significantly increased in comparison with naïve eyes and OHT eyes ($p<0.01$ Mann Whitney U test and $p<0.05$, Wilcoxon W test, respectively). No significant differences were found between OHT and naïve eyes (Fig. 13).

3.4.5. Quantification of cell body area of Iba-1+ cells in OPL, IPL and NFL-GCL

Iba-1+ cells in the OPL, IPL and NFL-GCL layers of OHT eyes showed significantly larger cell body areas than the corresponding cells in contralateral and naïve eyes ($p<0.001$, Mann Whitney U test; Fig. 14).

4. Discussion

Our results demonstrate that at 24 h after unilateral laser-induced OHT the microglia in all retinal layers showed multiple signs of reactivation such as migration, enlarged cell body area, shortening and reorientation of the processes, radial disposition of the soma and processes, and presence of amoeboid cells in both OHT eyes and their contralateral normotensive eyes (Fig. 15). However, the number of microglial Iba-1+ cells in the IPL, OPL, and OS showed no significant differences either in OHT eyes or in contralateral eyes compared with naïve eyes. Thus, at this time after OHT laser induction (24 h) a non-proliferative microglial reactivation was under way, a fact that could be due to an early reactivation stage. By contrast, in the same OHT experimental model at 15 days after OHT induction, a proliferative microglial reactivation was detected in the same retinal layers analyzed here (Rojas et al., 2014). No available studies in experimental models of OHT in mice have quantified retinal microglial cell number at early time periods (24 h) after OHT induction. Only one study has analyzed the number of microglial cells 2 h after OHT induction by the cauterization of the episcleral vein in rats, showing a significant increase of Iba-1+ cells through the retinal layers, mainly in the GCL and OPL (Wang et al., 2000). In addition, Zhang et al. reported an

increase in OX-42 and ED-1 microglial cells in the rat retina at 24 h after an acute increase in intraocular pressure (Zhang et al., 2005).

In our study, 24h post OHT laser induction, microglia migrate leaving areas of varying cell density in all retinal layers. In order to obtain representative results of the cell number in the retinal layers, we need to count cells in an extremely large number of retinal zones, which led us to develop an automated program for cell quantification in the plexiform layers (de Gracia et al., 2015). Unfortunately, this program cannot differentiate Iba-1+ cell morphologies and therefore cannot be used to obtain counts of Iba-1+ cells depending on their phenotype. This is a weakness of the present study.

In the NFL-GCL 24 h after lasering, similarly to that reported 15 days after unilateral laser-induced OHT (Rojas et al., 2014), we observed a significant increase in the area of the retina occupied by Iba-1+ cells (Iba1-RA) both in contralateral and OHT eyes. This increase could be caused by: i) the significant enlargement of the Iba-1+ cell body area relative to the cell body area in naivë eyes, ii) a greater number of Iba-1+ cells in this layer due to the entry of other non-microglial cell lines from the bloodstream; or iii) ramified Iba-1+ cells that have migrated to this layer from the IPL. Since no increase was found in the Iba-1+ cell number in the other retinal layers, the increase in Iba1-RA was probably not caused by microglial proliferation. By contrast, in a rat model of OHT by cauterization of the scleral veins, in which IOP values were similar to those found in our model, at 2 h after OHT induction the number of OX-42+ microglial cells was found to increase marginally in the contralateral retinas and throughout the retinal layers in the OHT, mostly in the GCL and OPL. (Wang et al., 2000).

At 24 h after ischemia, in an experimental model of acute OHT (saline injection in the anterior chamber at 120 mmHg for 60 min) (Zhang et al., 2005), there was a significant infiltration of round OX-42+, ED1+ (CD-68) and OX-6+ (MHC-II) cells with loss of the cell processes in the inner retina. In the present work, we also found Iba-1+ MHC-II+ rounded cells 24 h after lasering, mainly in the NFL-GCL near the optic disc and in the areas of Iba-1+ cell scarcity. These cells were located mostly close to the vessels, perhaps indicating that rounded cells could be coming from the bloodstream because of a possible blood retinal barrier (BRB) rupture, caused by the OHT. Although some round cells were seen in the contralateral eye, these were very scarce. In the central nervous system, at 24 h after ischemia, when the blood-brain barrier is compromised, round blood monocytes infiltrate the brain tissue (Gliem et al., 2012). In addition, it has been observed that the BRB is more permeable in the early stages of inflammatory processes.(Forrester et al., 2010; Xu et al., 2004). The above could explain the presence of abundant rounded Iba-1+ MHC-II+ cells observed in our study at such an early time after the OHT induction.

In addition, the Iba-1+ MHC-II+ dendritic like cells, professional antigen-presenting cells identified on the basis of MHC II co-localization, were more frequently observed both in OHT and in contralateral eyes than in naïve eyes. These cells were located near the collecting tube venule and forming rows of cells parallel to the vessels that emerged from the optic disc (Xu et al., 2007; Forrester et al., 2010). These locations could suggest a reinforcement in the surveillance of the BRB zones, which could be weakening after the IOP increase. The findings related to rounded cells and dendritic-like cells mentioned above, have been

642 observed in the same experimental model of OHT used here at 15 days after
643 OHT induction (Gallego et al., 2012; Rojas et al., 2014).

644 At 24 h after lasering, in the NFL-GCL, macrophagic amoeboid Iba-1+cells
645 containing abundant MHC-II+ vesicles were found near rounded MCH-II+ cells,
646 which could indicate a phagocytosis process. The ramified microglial cells of NFL-
647 GCL were catching rounded cells with their processes. The rounded MHC-II+
648 cells could be triggering the transformation of ramified microglial cells into
649 macrophagic amoeboid forms, which would phagocytose the rounded MHC-II+
650 cells. Accordingly, at 15 days after unilateral laser-induced OHT, in the NFL-CGL
651 and in OS, amoeboid CD68+ Iba-1+ microglia were also seen, mainly in OHT
652 eyes (Rojas et al., 2014). However, Wang et al. did not find macrophagic
653 ED1(CD-68)+ cells in OHT and contralateral retinas at 2 h after cauterizing
654 episcleral veins, suggesting that active phagocytosis were not involved in OHT-
655 derived changes at this early time (Wang et al., 2000).

656 Microglial cells were homogeneously distributed throughout the retina in naïve
657 and contralateral eyes. However, at 24 h after lasering a remarkable finding in all
658 OHT retinas studied was the presence of areas of Iba-1+ cell scarcity. Several
659 observations lead us to conclude that these areas were not due to tissue loss or
660 damage. First, they were found only in OHT eyes, not in naïve eyes or
661 contralateral eyes. In all instances, cell scarcity was uniform, it involved all retinal
662 layers and it localized consistently to the same retinal regions, mainly in the
663 superior retina. Second, the predominant cell morphology at the boundary of
664 areas of cell scarcity was a microglial amoeboid shape, with a branching
665 phenotype increasing towards the central retina. The apparent scarcity may also
666 reflect the retraction of major processes that made amoeboid cells smaller and

667 that created microglia-free spaces in the retina. Third, double immunostaining
668 with anti-Iba-1 and anti-GFAP showed that in OHT eyes, the astroglial plexus was
669 preserved in the areas of microglial cell scarcity (Supplementary Figure).

670 Next to the areas of Iba-1+ cell scarcity were zones of accumulation of rounded
671 MHC-II+ cells. The major concentration of rounded MHC-II+ cells in the superior
672 zone, could be related to a retinal area more sensitive to damage. In the
673 experimental model of OHT used in the present work, at 8 days after OHT
674 induction, 100% of the retinas analyzed showed areas lacking RCGs back
675 labeled with OHSt in the superior zone of the retina (Salinas-Navarro et al., 2009).
676 It has been demonstrated that at 24 h post-laser induction of OHT, there was a
677 significant reduction in the registered ERG waves, including positive STR, a- and
678 b-waves (Salinas-Navarro et al., 2009). The idea that areas of Iba-1+ cell scarcity
679 could represent zones of retinal damage is supported by the finding that those
680 ramified cells of the IPL and OPL located at the border of the areas of Iba-1+ cell
681 scarcity reorient their processes toward them. Rapid process extension and
682 reorientation towards the site of injury appear to be the initial responses of
683 microglia to injury (Walker et al., 2013). In the present work, we found scarce rod-
684 like microglia in the NFL-GCL unlike the large number of them found in the OHT
685 eyes 15 days after laser induction (de Hoz et al., 2013) where most of the RGCs
686 are lost (Salinas-Navarro et al., 2009). Rod-like microglia are related to axonal
687 injury (Ziebell et al., 2012). Thus, the scarcity of rod-like microglia in the present
688 work could indicate that 24 h after OHT induction, widespread axonal damage
689 would not yet have occurred.

690 On the other hand, remarkable morphological signs of reactivation observed at
691 24 h after unilateral laser-induced OHT was the shortening of microglial

692 processes, enlargement of the cell body and the transformation of these cells into
693 a macrophage-like morphology, known as amoeboid microglia, mainly in the OHT
694 eyes (Fig. 15). This process shortening could be consistent with the significant
695 reduction of the Iba-1+ cell-arbor area found in OHT eyes with respect to
696 contralateral and naïve eyes in the IPL, and in the OHT eyes with respect to naïve
697 eyes in the OPL. The amoeboid microglia was found in the NFL-GCL and the OS.
698 This microglial phenotype represents a state of high reactivity where the cells act
699 as macrophages, engulfing and destroying cell debris (Streit et al., 1999). In the
700 OHT retinas, many amoeboid microglia showed vacuoles inside, some of which
701 contained MHC-II+ cells debris. In addition, in the surface and in the proximity of
702 some amoeboid microglias, we observed small Iba-1+ vesicles, which could
703 correspond to extracellular vesicles. These vesicles are important mediators of
704 intercellular communication and can be produced by microglial cells. They are
705 involved in all immune activities and their effect in neurodegenerative disorders
706 can be protective or detrimental. (Robbins and Morelli, 2014; Joshi et al., 2015;
707 Nigro et al., 2016).

708 Another morphological type of microglial cell observed at 24 h after OHT induction
709 was the dystrophic microglia. These cells were found mainly in the OS both in
710 OHT and in contralateral eyes. Although dystrophic microglia are related to
711 chronic stress that contributes to exhaustion and senescence of the microglia,
712 acute injury inducing intense inflammation may accelerate the natural
713 senescence process of microglial cells, and dystrophic microglia may appear
714 (Streit et al., 2014). In the IPL, some ramified microglial cells located near to the
715 areas of Iba-1+ cell scarcity showed beaded fragmenting processes and

716 spheroids. These cells could correspond to an early phase of dystrophic microglia
717 (Nigro et al., 2016; Streit et al., 2014).

718 In the present study, other remarkable features of the retinal microglia both in
719 contralateral eyes and in OHT eyes were the shift of some ramified Iba-1+ cells
720 in the plexiform layers from a parallel to a radial disposition with respect to the
721 retinal surface (Fig. 15). This shift was more frequently noted in OHT eyes. These
722 radial cells sent processes toward the neighboring layers, connecting several
723 retinal layers between them (Fig. 15). Radial microglial has also been found at 15
724 days after OHT laser induction (Rojas et al., 2014), in a hereditary glaucoma
725 model DBA/2J (D2) (Bosco et al., 2011), and in retinal degeneration (Karlstetter
726 et al., 2015). This radial arrangement, similar to that of Müller's glia, could
727 contribute to the distribution of signaling between the different microglial
728 plexuses. In addition, it could play an important role in the transmission of the
729 information, from the layers where the BRB could be impaired to the rest of the
730 retinal layers. In the OPL and IPL, some of the ramified microglial cells moved
731 and reoriented their processes toward radial cells surrounding them, possibly to
732 communicate. This could explain the alteration in the pattern of the cell mosaic in
733 the plexiform layers with sectorial microglia accumulation.

734 At 24 h after lasering, it was notable in the contralateral eye that microglial cells
735 of IPL, OPL, and OS sent numerous vertical processes to the neighboring retinal
736 layer (Fig. 15). We detected a significant increase in the number of radial
737 microglial processes connecting the OPL and OS (the only retinal area in which
738 their quantification was possible due to retinal structure) in comparison with naïve
739 and OHT eyes. Vertical microglial processes connected several retinal layers,
740 probably in an attempt of very early communication between the microglial

plexuses after the OHT induction, and could play a role in the early signaling microglial reactivation. Notably, at 15 days of OHT laser induction (Rojas et al., 2014), the vertical microglial processes in contralateral eyes were less frequently observed than at 24 h after lasering.

One of the most noteworthy observations of this work was the early activation (24h after lasering) of microglial cells in normotensive contralateral eyes (Fig. 15). This early microglial activation could be mediated by the immune system. BRB impairment in the OHT eyes could be a key mechanism for triggering the immune response that can induce the early microglial activation in the contralateral eye.

5. CONCLUSIONS

In this study, we report for the first time, descriptively and quantitatively, the early behavior of mouse retinal microglial cells at 24 h after unilateral laser-induced OHT. Our data support the contention that early after OHT-induction both treated as well as contralateral untreated eyes showed a non-proliferative microglial reactivation, more pronounced in OHT eyes. This reactivation was characterized by (Fig. 15): enlarged cell body area, cell movement, high degree of branching, shortening and reorientation of the processes, presence of amoeboid microglia acting as a macrophages, and radial disposition of the soma and processes toward adjacent microglial plexuses which could be contributing to signaling communication between the different microglial layers. The presence of rounded cells could be related to BRB disruption, contributing to microglial reactivation. The early microglial reactivation, both in OHT and contralateral eye, could support the implication of the immune system in the context of OHT-related neurodegeneration.

Acknowledgements: The authors would like to thanks Desireé Contreras for technical assistance. David Nesbitt corrected the English version of this work.

References

Blinzinger, K., Kreutzberg, G., 1968. Displacement of synaptic terminals from regenerating motoneurons by microglial cells. Cell Tissue Res. 85, 145-157.

Bodeutsch, N., Siebert, H., Dermon, C., Thanos, S., 1999. Unilateral injury to the adult rat optic nerve causes multiple cellular responses in the contralateral site. J. Neurobiol. 38, 116-128.

Bosco, A., Inman, D.M., Steele, M.R., Wu, G., Soto, I., Marsh-Armstrong, N., Hubbard, W.C., Calkins, D.J., Horner, P.J., Vetter, M.L., 2008. Reduced retina microglial activation and improved optic nerve integrity with minocycline treatment in the DBA/2J mouse model of glaucoma. Invest. Ophthalmol. Vis. Sci. 49, 1437-1446.

Bosco, A., Steele, M.R., Vetter, M.L., 2011. Early microglia activation in a mouse model of chronic glaucoma. J. Comp. Neurol. 519, 599-620.

Bosco, A., Crish, S.D., Steele, M.R., Romero, C.O., Inman, D.M., Horner, P.J., Calkins, D.J., Vetter, M.L., 2012. Early reduction of microglia activation by irradiation in a model of chronic glaucoma. PLoS One 7, e43602.

Cuenca, N., Pinilla, I., Fernández-Sánchez, L., Salinas-Navarro, M., Alarcón-Martínez, L., Avilés-Trigueros, M., de la Villa, P., Miralles de Imperial, J., Villegas-Pérez, M.P., Vidal-Sanz, M., 2010. Changes in the inner and outer retinal layers after acute increase of the intraocular pressure in adult albino Swiss mice. Exp. Eye Res. 91, 273-285.

Davis, B.M., Salinas-Navarro, M., Cordeiro, M.F., Moons, L., Groef, L., 2017. Characterizing microglia activation: a spatial statistics approach to maximize information extraction. Sci. Rep. 7, 1576-017-01747-8.

de Gracia, P., Gallego, B.I., Rojas, B., Ramirez, A.I., de Hoz, R., Salazar, J.J., Trivino, A., Ramirez, J.M., 2015. Automatic Counting of Microglial Cells in Healthy and Glaucomatous Mouse Retinas. PLoS One 10, e0143278.

de Hoz, R., Gallego, B.I., Ramírez, A.I., Rojas, B., Salazar, J.J., Valiente-Soriano, F.J., Avilés-Trigueros, M., Villegas-Perez, M.P., Vidal-Sanz, M., Triviño, A., 2013. Rod-Like Microglia Are Restricted to Eyes with Laser-Induced Ocular Hypertension but Absent from the Microglial Changes in the Contralateral Untreated Eye. PLoS ONE 8, e83733.

Forrester, J.V., Xu, H., Kuffova, L., Dick, A.D., McMenamin, P.G., 2010. Dendritic cell physiology and function in the eye. Immunol. Rev. 234, 282-304.

Fu, C.T., Sretavan, D., 2010. Laser-Induced Ocular Hypertension in Albino CD-1 Mice. Invest. Ophthalmol. Vis. Sci. 51, 980-990.

Gallego, B.I., Salazar, J.J., de Hoz, R., Rojas, B., Ramírez, A.I., Salinas-Navarro, M., Ortín-Martínez, A., Valiente-Soriano, F.J., Avilés-Trigueros, M., Villegas-Perez, M.P., 2012. IOP induces upregulation of GFAP and MHC-II and microglia reactivity in mice retina contralateral to experimental glaucoma. J. Neuroinflammation. 9, 92.

Gallego, B.I., de Gracia, P., 2016. Automatic counting of microglial cell activation and its applications. Neural Regen. Res. 11, 1212-1215.

Gliem, M., Mausberg, A.K., Lee, J.I., Simiantonakis, I., van Rooijen, N., Hartung, H.P., Jander, S., 2012. Macrophages prevent hemorrhagic infarct transformation in murine stroke models. Ann. Neurol. 71, 743-752.

Ha, Y., Liu, H., Xu, Z., Yokota, H., Narayanan, S.P., Lemtalsi, T., Smith, S.B., Caldwell, R.W., Caldwell, R.B., Zhang, W., 2015. Endoplasmic reticulum stress-regulated CXCR3 pathway mediates inflammation and neuronal injury in acute glaucoma. Cell. Death Dis. 6, e1900.

Inman, D.M., Horner, P.J., 2007. Reactive nonproliferative gliosis predominates in a chronic mouse model of glaucoma. Glia 55, 942-953.

Joshi, P., Benussi, L., Furlan, R., Ghidoni, R., Verderio, C., 2015. Extracellular vesicles in Alzheimer's disease: friends or foes? Focus on abeta-vesicle interaction. Int. J. Mol. Sci. 16, 4800-4813.

Karlstetter, M., Scholz, R., Rutar, M., Wong, W.T., Provis, J.M., Langmann, T., 2015. Retinal microglia: Just bystander or target for therapy? Prog. Retin. Eye Res. 45, 30-57.

Kettenmann, H., Hanisch, U., Noda, M., Verkhratsky, A., 2011. Physiology of Microglia. Physiological Reviews 91, 461-553.

Kezic, J.M., Chrysostomou, V., Trounce, I.A., McMenamin, P.G., Crowston, J.G., 2013. Effect of anterior chamber cannulation and acute IOP elevation on retinal macrophages in the adult mouse. Invest Ophthalmol Vis Sci 54, 3028-3036.

Levkovitch-Verbin, H., Kalev-Landoy, M., Habot-Wilner, Z., Melamed, S., 2006. Minocycline delays death of retinal ganglion cells in experimental glaucoma and after optic nerve transection. Arch. Ophthalmol. 124, 520-526.

Liu, S., Li, Z., Weinreb, R.N., Xu, G., Lindsey, J.D., Ye, C., Yung, W., Pang, C., Lam, D.S.C., Leung, C.K., 2012. Tracking Retinal Microgliosis in Models of Retinal Ganglion Cell Damage. Invest Ophthalmol Vis Sci 53, 6254-6262.

838 Luo, X., Ding, J., Chen, S., 2010. Microglia in the aging brain: relevance to
839 neurodegeneration. Molecular Neurodegeneration 5, 12.

840 Madeira, M.H., Boia, R., Santos, P.F., Ambrosio, A.F., Santiago, A.R., 2015.
841 Contribution of microglia-mediated neuroinflammation to retinal degenerative
842 diseases. Mediators Inflamm. 2015, 673090.

843 Naskar, R., Wissing, M., Thanos, S., 2002. Detection of early neuron
844 degeneration and accompanying microglial in the retina of a rat model of
845 glaucoma. Invest Ophthalmol Vis Sci 43, 2962-2968.

846 Neufeld, A.H., 1999. Microglia in the optic nerve head and the region of
847 parapapillary chorioretinal atrophy in glaucoma. Arch. Ophthalmol. 117, 1050-
848 1056.

849 Nigro, A., Colombo, F., Casella, G., Finardi, A., Verderio, C., Furlan, R., 2016.
850 Myeloid Extracellular Vesicles: Messengers from the Demented Brain. Front.
851 Immunol. 7, 17.

852 Quigley, H.A., Broman, A.T., 2006. The number of people with glaucoma
853 worldwide in 2010 and 2020. Brit. J. Ophthalmol. 90, 262-267.

854 Quigley, H.A., 1983. Experimental glaucoma damage mechanism. Arch.
855 Ophthalmol. 101, 1301-1302.

856 Quigley, H.A., Hohman, R.M., 1983. Laser energy levels for trabecular
857 meshwork damage in the primate eye. Invest. Ophthalmol. Vis. Sci. 24, 1305-
858 1307.

859 Ramírez, A., Rojas, B., de Hoz, R., Salazar, J., Gallego, B., Triviño, A.,
860 Ramírez, J., 2015. Microglia, inflammation, and glaucoma. In: Glaucoma. SM
861 Group Open Access eBooks Dover USA. 2015.
862 http://www.smgebooks.com/glaucoma/chapters/GLC-15-02.pdf

863 Ramírez, A.I., Salazar, J.J., de Hoz, R., Rojas, B., Gallego, B.I., Salinas-
864 Navarro, M., Alarcón-Martínez, L., Ortín-Martínez, A., Avilés-Trigueros, M.,
865 Vidal-Sanz, M., Trivino, A., Ramírez, J.M., 2010. Quantification of the effect of
866 different levels of IOP in the astroglia of the rat retina ipsilateral and
867 contralateral to experimental glaucoma. Invest. Ophthalmol. Vis. Sci. 51, 5690-
868 5696.

869 Ransohoff, R.M., Perry, V.H., 2009. Microglial physiology: unique stimuli,
870 specialized responses. Annu. Rev. Immunol. 27, 119-145.

871 Robbins, P.D., Morelli, A.E., 2014. Regulation of immune responses by
872 extracellular vesicles. Nat. Rev. Immunol. 14, 195-208.

873 Rojas, B., Gallego, B.I., Ramírez, A.I., Salazar, J.J., de Hoz, R., Valiente-
874 Soriano, F.J., Avilés-Trigueros, M., Villegas-Perez, M.P., Vidal-Sanz, M.,
875 Triviño, A., 2014. Microglia in mouse retina contralateral to experimental

glaucoma exhibit multiple signs of activation in all retinal layers. J. Neuroinflammation. 11, 133.

Salinas-Navarro, M., Alarcon-Martinez, L., Valiente-Soriano, F.J., Ortin-Martinez, A., Jimenez-Lopez, M., Aviles-Trigueros, M., Villegas-Perez, M.P., de la Villa, P., Vidal-Sanz, M., 2009. Functional and morphological effects of laser-induced ocular hypertension in retinas of adult albino Swiss mice. Mol. Vis. 15, 2578-2598.

Shimazawa, M., Yamashima, T., Agarwal, N., Hara, H., 2005. Neuroprotective effects of minocycline against in vitro and in vivo retinal ganglion cell damage. Brain Res. 1053, 185-194.

Streit, W.J., Conde, J.R., Fendrick, S.E., Flanary, B.E., Mariani, C.L., 2005. Role of microglia in the central nervous system's immune response. Neurol. Res. 27, 685-691.

Streit, W.J., Xue, Q.S., Tischer, J., Bechmann, I., 2014. Microglial pathology. Acta Neuropathol. Commun. 2, 142.

Streit, W.J., Walter, S.A., Pennell, N.A., 1999. Reactive microgliosis. Progress in Neurobiology 57, 563-581.

Tezel, G., the Fourth ARVO/Pfizer Ophthalmics Research Institute Conference,Working Group, 2009. The role of glia, mitochondria, and the immune system in glaucoma. Invest Ophthalmol Vis Sci 50, 1001-1012.

Trapp, B.D., Wujek, J.R., Criste, G.A., Jalabi, W., Yin, X., Kidd, G.J., Stohlman, S., Ransohoff, R., 2007. Evidence for synaptic stripping by cortical microglia. Glia 55, 360-368.

Triviño, A., Ramírez, J.M., Ramírez, A.I., Salazar, J.J., García-Sánchez, J., 1992. Retinal perivascular astroglia: an immunoperoxidase study. Vision Res. 32, 1601-1607.

Triviño, A., De Hoz, R., Salazar, J.J., Ramírez, A.I., Rojas, B., Ramírez, J.M., 2002. Distribution and organization of the nerve fiber and ganglion cells of the human choroid. Anat. Embryol. (Berl) 205, 417-430.

Trost, A., Motloch, K., Bruckner, D., Schroedl, F., Bogner, B., Kaser-Eichberger, A., Runge, C., Strohmaier, C., Klein, B., Aigner, L., Reitsamer, H.A., 2015. Time-dependent retinal ganglion cell loss, microglial activation and blood-retina-barrier tightness in an acute model of ocular hypertension. Exp. Eye Res. 136, 59-71.

Walker, F.R., Nilsson, M., Jones, K., 2013. Acute and chronic stress-induced disturbances of microglial plasticity, phenotype and function. Curr. Drug Targets 14, 1262-1276.

913 Wang, K., Peng, B., Lin, B., 2014. Fractalkine receptor regulates microglial
914 neurotoxicity in an experimental mouse glaucoma model. Glia 62, 1943-1954.

915 Wang, X., Tay, S., Ng, Y.K., 2000. An immunohistochemical study of neuronal
916 and glial cell reactions in retinae of rats with experimental glaucoma. Exp. Brain
917 Res. 132, 476.

918 Wang, J., Valiente-Soriano, F.J., Nadal-Nicolas, F.M., Rovere, G., Chen, S.,
919 Huang, W., Agudo-Barriuso, M., Jonas, J.B., Vidal-Sanz, M., Zhang, X., 2017.
920 MicroRNA regulation in an animal model of acute ocular hypertension. Acta
921 Ophthalmol. 95, e10-e21.

922 Xu, H., Manivannan, A., Goatman, K.A., Jiang, H.R., Liversidge, J., Sharp, P.F.,
923 Forrester, J.V., Crane, I.J., 2004. Reduction in shear stress, activation of the
924 endothelium, and leukocyte priming are all required for leukocyte passage
925 across the blood--retina barrier. J. Leukoc. Biol. 75, 224-232.

926 Xu, H., Dawson, R., Forrester, J.V., Liversidge, J., 2007. Identification of novel
927 dendritic cell populations in normal mouse retina. Invest. Ophthalmol. Vis. Sci.
928 48, 1701-1710.

929 Yuan, L., Neufeld, A.H., 2001. Activated microglia in the human glaucomatous
930 optic nerve head. J. Neurosci. Res. 64, 523-532.

931 Zhang, C., Lam, T.T., Tso, M.O., 2005. Heterogeneous populations of
932 microglia/macrophages in the retina and their activation after retinal ischemia
933 and reperfusion injury. Exp. Eye Res. 81, 700-709.

934 Ziebell, J.M., Taylor, S.E., Cao, T., Harrison, J.L., Lifshitz, J., 2012. Rod
935 microglia: elongation, alignment, and coupling to form trains across the
936 somatosensory cortex after experimental diffuse brain injury.
937 J.Neuroinflammation 9, 247.

938

939

940

Figure captions

Figure 1. Methodology for Iba-1+ cell quantification

(A) Illustration of retinal whole-mount showing areas of retina selected for quantitative analysis of Iba-1+ cells toward the horizontal and vertical meridian. (B) Work flow describing the algorithm for Iba-1+ microglial cell counting. (1) Sets of images are taken by scanning a layer of the retina every 2 μm in depth (Z direction). The averaged image of the set of images taken in depth is the Z projection (2); afterward, image thresholding (3) and segmentation (4) into 50×50-pixel regions of interest are performed. Examples of correct cell identification and multiple identification of the same cell in various segments (6 inset) and final detection of cells (6). (C) Retinal area labeled with Iba-1 in the NFL-GCL. Left panel shows a microphotograph from the NFL-GCL. Right panel shows the same image after thresholding. The percentage of retinal area labeled with Iba-1 in this example is 7.2%. Modified from de Gracia et al. (de Gracia et al., 2015). Used with permission from Barrow Neurological Institute, Phoenix, Arizona.

Figure 2. Iba-1+ microglia unevenly distributed in OHT retinas at 24 hours after lasering.

Retinal whole-mounts. Iba-1 immunostaining. In contralateral eyes (A) Iba-1+ cells were distributed in a mosaic of tiled cells that built a network throughout the retina. In OHT eyes (B, C) this network was not homogeneous. Mainly in the peripheral superior area of the retina (C), there were areas of Iba-1+ cell scarcity (arrow in B) in which the microglial cells even disappeared. The dotted line in B represents the boundary of peripheral areas of cell scarcity. [I: inferior zone; N:

964 nasal zone; S: superior zone; T: temporal zone; OD: optic disc; OHT: ocular
965 hypertension].

966 **Figure 3. Iba-1+ cells in the NFL-GCL at 24 hours after unilateral laser-**
967 **induced OHT.**

968 Retinal whole-mounts. Iba-1 immunostaining. In naïve eyes (A, B) there were
969 ramified Iba-1+ cells (open arrowhead in A) and perivascular Iba-1+ cells
970 (arrowhead in B). Both in contralateral eyes (C, D) and in OHT eyes (E-F) ramified
971 Iba-1+ cells and perivascular Iba-1+cells showed an enlargement of the cell body
972 (open arrowhead in C, E and arrowhead in D, F) and retraction of the cell
973 processes, as shown by the reduction of the area encircled by the solid line
974 surrounding Iba-1+ cells (A,C,E) [NFL-GCL: nerve fiber layer-ganglion cell layer;
975 OHT: ocular hypertension; v: retinal vessel].

976 **Figure 4. Additional morphological types of Iba-1+ cells in the NFL-GCL at**
977 **24 hours after unilateral laser-induced OHT.**

978 Retinal whole-mounts. Iba-1 immunostaining (A-H). MHC-II immunostaining (H-
979 I). In contralateral eyes (A,B), in addition to ramified Iba-1+ cells scarce amoeboid
980 Iba-1+ cells (arrowhead in B) were also observed. In OHT eyes, the shortening
981 of the processes in ramified Iba-1+ cells were notable (C). Amoeboid Iba-1+ cells
982 (arrowhead in E) were abundant in OHT eyes, mainly close to the areas of Iba-
983 1+ cell scarcity (asterisk). Some amoeboid Iba-1+ cells had vacuoles inside
984 (arrow in D) and small vesicles in the surface (arrowhead in D) and in the vicinity
985 of the cell (open arrowhead in D). Only in OHT eyes three additional
986 morphological types of Iba-1+ cells were discerned: rod-like cells with elongated
987 cell bodies and two processes prominently projecting from each pole (arrows in

F); ramified Iba-1+ cells showing a morphology similar to those observed in the IPL, suggesting that these cells had migrated to this layer from the IPL (arrowhead in G); and dendritic Iba-1+ cells which expressed MHC-II (arrow in H,I). [NFL-GCL: nerve fiber layer-ganglion cell layer; OHT: ocular hypertension].

Figure 5. Relationship between ramified Iba-1+ cells and rounded MHC-II+ cells in the NFL-GCL at 24 hours after unilateral laser-induced OHT.

Retinal whole-mounts. Iba-1 immunostaining (A,C). MHC-II immunostaining (A-D). Ramified Iba-1+ cells seem to catch the rounded cells with their processes in contralateral (arrow in A) and OHT eyes (arrows in C) being scarce in the former. Rounded cells express MHC-II (arrows in B,D). [NFL-GCL: nerve fiber layer-ganglion cell layer; OHT: ocular hypertension].

Figure 6. Rounded MHC-II+ cell distribution in the NFL-GCL at 24 hours after unilateral laser-induced OHT.

Retinal whole-mounts. Iba-1 immunostaining (A,C,E,G). MHC-II immunostaining (A-H). Rounded MHC-II+ cells (arrows in A-F) were frequently observed in the retinal periphery close to the areas of Iba-1+ cell scarcity (A-D) as shown above the dotted line, and near the optic disk (arrows in E,F). Amoeboid Iba-1+ cells had MHC-II + vacuoles inside (G,H). (NFL-GCL: nerve fiber layer-ganglion cell layer; OD: optic disk; OHT: ocular hypertension; S: superior).

Figure 7. Iba-1+ cells in the IPL at 24 hours after unilateral laser-induced OHT.

Retinal whole-mounts. Iba-1 immunostaining (A-H). MHC-II immunostaining (F-K). In naïve, Iba-1+ cells were ramified and formed a regular mosaic (arrowhead

in A). In addition, there were few Iba-1+ MHC-II+ cells with a dendritic-like appearance (F, I). In comparison with naïve eyes (A), ramified Iba-1+ cells of contralateral eyes and OHT eyes (arrowheads in B and C respectively) showed enlargement of the cell body. In both eyes the distribution throughout the retina in a mosaic–like fashion observed in naïve eyes (A) was disrupted due to microglia migration to form clusters (encircled cells in B and C), leaving free Iba-1+ cells spaces around them. This trend was more evident in OHT eyes (C) than in contralateral eyes (B). In OHT eyes ramified Iba-1+ cells reoriented their processes (arrowhead in D) toward the areas of Iba-1+ cell scarcity (asterisk in D). Some of these cells were thicker and presented spheroidal swelling (arrow in E). The Iba-1+ MHC-II+ dendritic-like cells were most frequently found in contralateral (G,J) and OHT eyes (H,K) than in naïve (F,I). (IPL: inner plexiform layer; OHT: ocular hypertension).

Figure 8. Iba-1+ cells in the OPL at 24 hours after unilateral laser-induced OHT.

Retinal whole-mount (A-H). Iba-1 immunostaining (A-H). Cut-view analysis in the YZ plane (E,H). In comparison with naïve eyes (A), the regular mosaic formed by ramified Iba-1+ cells (arrowhead) was lost in some areas of contralateral (B, D) and OHT (C) eyes, this being more pronounced in the later, due to the presence of radial Iba-1+ cells (arrow in C, D) and the approach of the processes of ramified cells toward them (C, D). Occasionally, the processes of two neighboring cells were so close together that no space between them was visible (arrow in F). In OHT (C,F) and contralateral eyes (B,D) ramified Iba-1+ cells (arrowhead) showed enlargement of the cell body and more secondary and superior order processes than in naïve (A). In contralateral eyes Iba-1+ cells of the OPL projected several

long processes (arrows in E) that reached the OS, some of them were located near Iba-1+ cells of the OS (arrowhead in E). In OHT eyes (G), the processes of ramified Iba-1+ cells (arrowheads) reoriented toward the areas of Iba-1+ cell scarcity (asterisk in G). Close to these ramified iba-1+cells, Iba-1+ radial cells (arrow in G, H) were observed. [OHT: ocular hypertension; OPL: outer plexiform layer, OS photoreceptor outer segment].

Figure 9. Iba-1+ cells between IPL- OPL- OS at 24 hours after unilateral laser-induced OHT.

Retinal whole-mount. Iba-1 immunostaining (A-C). Cut-view analysis in the YZ plane (A-C). Iba-1+ cells of IPL, OPL sent numerous processes (arrowhead) to the neighboring microglial plexuses mainly in contralateral eyes (A-C). Some Iba-1+ cells from IPL and OPL present a radial disposition (arrow) with their processes participating in the neighboring microglial plexuses; this was more evident in OHT eyes (C) than in contralateral eyes (A,B) (OHT: ocular hypertension; IPL: inner plexiform layer; OPL: outer plexiform layer; OS photoreceptor outer segment).

Figure 10. Iba-1+ cells in the OS at 24 hours after unilateral laser-induced OHT.

Retinal whole-mount. Iba-1 immunostaining (A-O). Cut-view analysis in the YZ plane (B,F,K,O). Type 1 (A,B) and Type 2 (C) Iba-1+ cells in the OS in naïve eyes. In Type 1-OS Iba-1+ cells numerous processes emerged from the same point of the soma, like the roots of a tree (A,B). As a result, Type 1-OS showed a radial disposition in the retina, and soma and processes were located on different Z planes. Therefore we preferred to assess morphological characteristics of Type

1-OS cells in cut-view analysis in the yz plane (AB). Cut-views showed that type 1-OS Iba-1+ cells extend across the thickness of the OS perpendicularly to the retinal surface. In comparison with naïve eyes (A,B), in contralateral eyes (D,E) and OHT eyes (arrowhead in L) Type 1-OS Iba-1+ cell changed their orientation from perpendicular to parallel to the retinal surface. Both in contralateral eyes (G) and in OHT eyes (M), Type 2-OS Iba-1+ cells (arrow) showed a retraction of their processes and a hairy appearance with respect to naïve eyes (C). The latter being due to abundant thin and short processes sprouting from the soma and main processes (G,M). Unlike naïve eyes, in contralateral eyes occasionally, a long cell process from a Type 1-OS Iba-1+ cell reached the OPL plexus (arrow in F). Type 1-OS Iba-1+ cell was the cell type most frequently observed in contralateral eyes (D,E). Additional morphological Iba-1+ cells were observed in contralateral and OHT eyes, amoeboid cells (arrows in H,L) and dystrophic cells (arrows in I,N). In OHT eyes, amoeboid cells and dystrophic cells were the predominant cell types. In contralateral eyes numerous processes from Iba-1+ cells of the OPL extended to the OS branching profusely (arrowheads in J,K). In OHT eyes radial cells from OPL reached the OS (arrows in O). [OHT: ocular hypertension; OPL: outer plexiform layer; OS photoreceptor outer segment].

Figure 11. Area of the retina occupied by Iba-1+ cells (Iba1-RA) in the NFL-GCL at 24 hours after unilateral laser-induced OHT.

Each bar represents the mean ± SD of the area of the retina occupied by Iba-1+ cells. **P <0.01 contralateral and OHT retinas vs. naive. *P <0.05 OHT retinas vs. contralateral retinas. [NFL-GCL: nerve fiber layer-ganglion cell layer; OHT: ocular hypertension; RA: retinal area].

Figure 12. Arbor area of Iba-1+ cells in the plexiform layers at 24 hours after unilateral laser-induced OHT.

Each bar represents the mean ± SD of the arbor area of the Iba-1+ cells. Dotted lines represent comparison among OPL values: *P <0.05 naïve vs. OHT retinas. Solid lines represent comparison among IPL values: *P <0.05 OHT retinas vs. contralateral and **P <0.01 vs. naïve retinas. [OHT: ocular hypertension; IPL: inner plexiform layer; OPL: outer plexiform layer].

Figure 13. Quantification of microglial vertical process between OPL and OS at 24 hours after unilateral laser-induced OHT.

Each bar represents the mean ± SD of microglial vertical processes between OPL and OS. **P <0.01 contralateral vs. naïve retinas. *P <0.05 contralateral vs. OHT retinas. [OHT: ocular hypertension]

Figure 14. Quantification of the cell body area of Iba-1+ cells in the OPL, IPL and NFL-GCL at 24 hours after unilateral laser-induced OHT.

Each bar represents the mean ± SD of the cell body area of Iba-1 + cells. **P <0.01 for contralateral and OHT retinas vs. naïve retinas. **P <0.01 for OHT retinas vs. contralateral retinas. [NFL-GCL: nerve fiber layer-ganglion cell layer; OHT: ocular hypertension; IPL: inner plexiform layer; OPL: outer plexiform layer].

Figure 15. Schematic representation of retinal microglial behavior at 24 hours after unilateral laser-induced OHT.

The drawing illustrate the disposition of microglial cells in the different retinal layers. In naïve eyes, the microglia have a “resting” phenotype and locate in the NFL-GCL, IPL, OPL and OS. In contralateral eyes the microglia acquire an

reactivated phenotype and send numerous processes to neighboring retinal layers in an attempt of early communication between retinal microglial plexuses. In OHT eyes, the microglial cells show a higher degree of reactivation than contralateral eyes. Some microglial cells of IPL and OPL acquire a radial disposition and send processes toward adjacent microglial plexuses. This radial arrangement of microglial cells can contribute to signaling communication between the different microglial layers. [NFL: nerve-fiber layer; GCL: ganglion cell layer; OHT: ocular hypertension; IPL: inner plexiform layer; OPL: outer plexiform layer; OS photoreceptor outer segment].

TABLES

Table 1. Iba-1+ cell quantification in the IPL, OPL, and OS.

	IPL	OPL	OS
NAIVE	15.87 ± 1,73	19.99 ± 2,31	1.44 ± 0.75
CONTRALATERAL	13.57 ± 2,17	20.25 ± 0,40	1.79 ± 1.08
OHT	11.02 ± 6,68	16.42 ± 3,86	4.00 ± 2.966

Data are presented as the mean number of Iba-1+ cells ± SD. Measurements were made at 20x, giving up an area of 0.1502 mm^2 per field analyzed. (IPL: inner plexiform layer; OHT: ocular hypertension; OPL: outer plexiform layer; OS: photoreceptor outer segment).

Highlights

- 24h after laser-induced OHT, a non-proliferative microglial reactivation was shown both in OHT eyes and their contralateral untreated eyes.
- This fast microglial activation in both eyes could be mediated by the immune system.

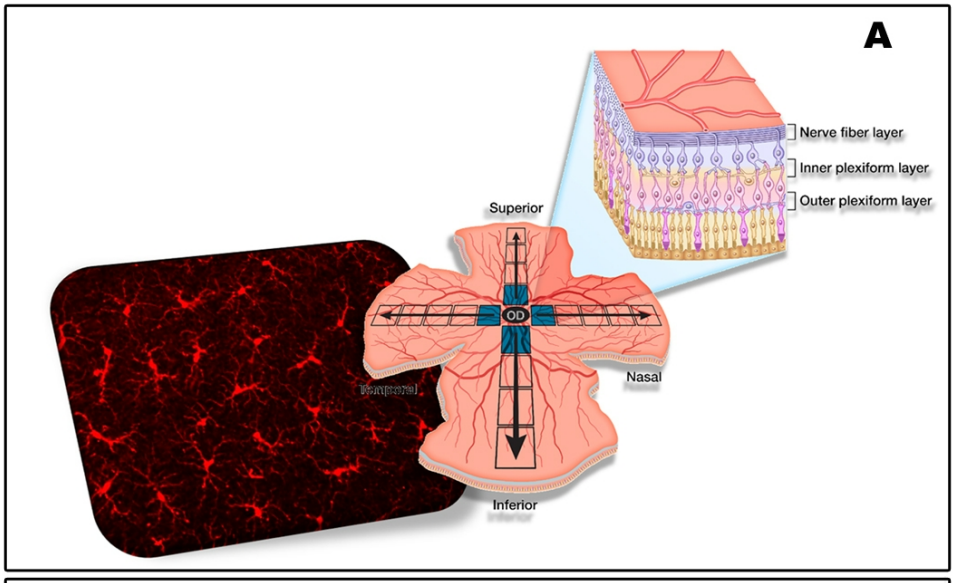
A
Nerve fiber layer
Inner plexiform layer
Outer plexiform layer
Superior
OD
Nasal
Temporal
Inferior

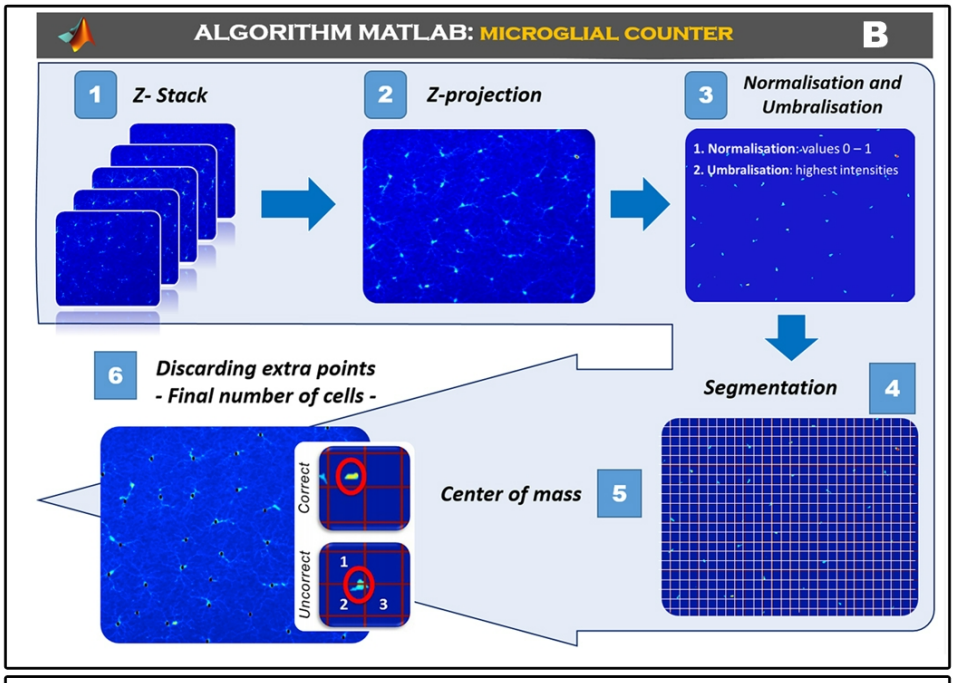
ALGORITHM MATLAB: MICROGLIAL COUNTER
B
1 Z- Stack
2 Z-projection
3 Normalisation and Umbralisation
1. Normalisation:-values 0 – 1
2. Umbralisation: highest intensities
Segmentation 4
Center of mass 5
6 Discarding extra points
- Final number of cells -
Correct
Uncorrect
1
2
3

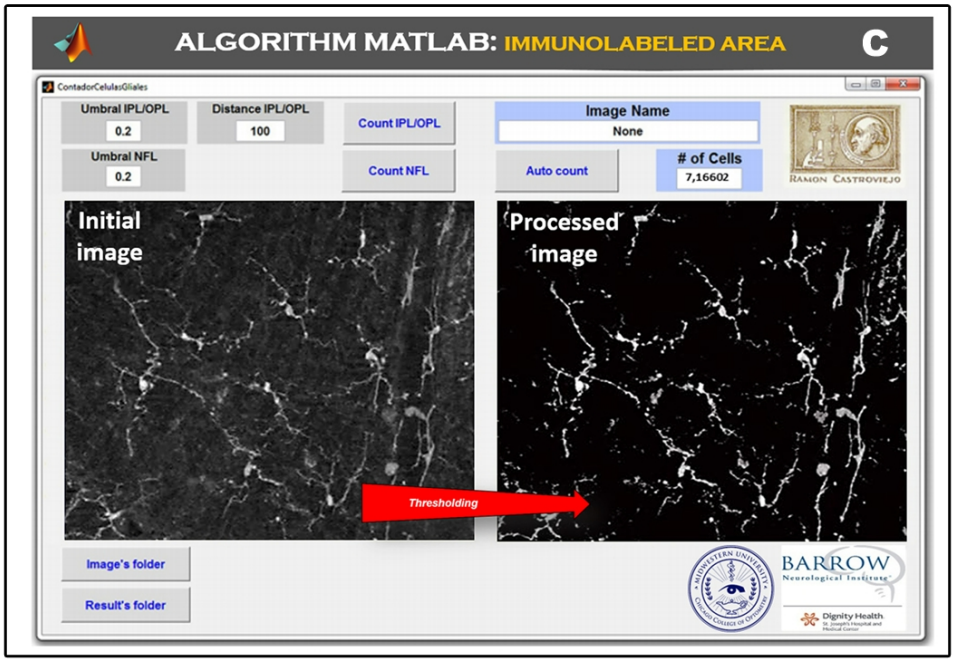
ALGORITHM MATLAB: IMMUNOLABELED AREA
C
ContadorCelulasGliales
Umbral IPL/OPL
0.2
Distance IPL/OPL
100
Count IPL/OPL
Image Name
None
Umbral NFL
0.2
Count NFL
Auto count
# of Cells
7,16602
Ramon Castroviejo
Initial image
Processed image
Thresholding
Image's folder
Result's folder
BARROW
Neurological Institute
Dignity Health

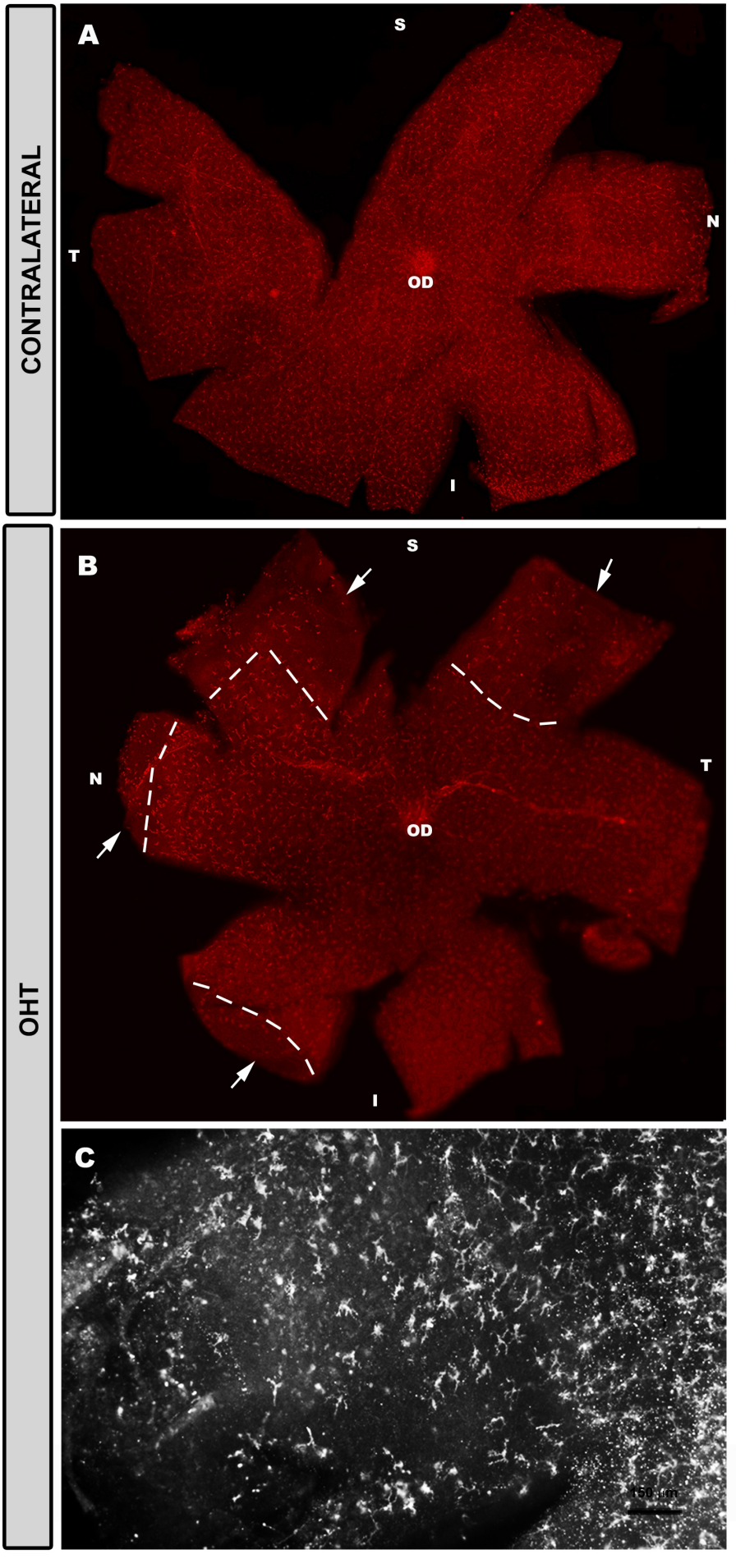
CONTRALATERAL
A
S
N
T
OD
I
OHT
B
S
N
T
OD
I
C
150 µm

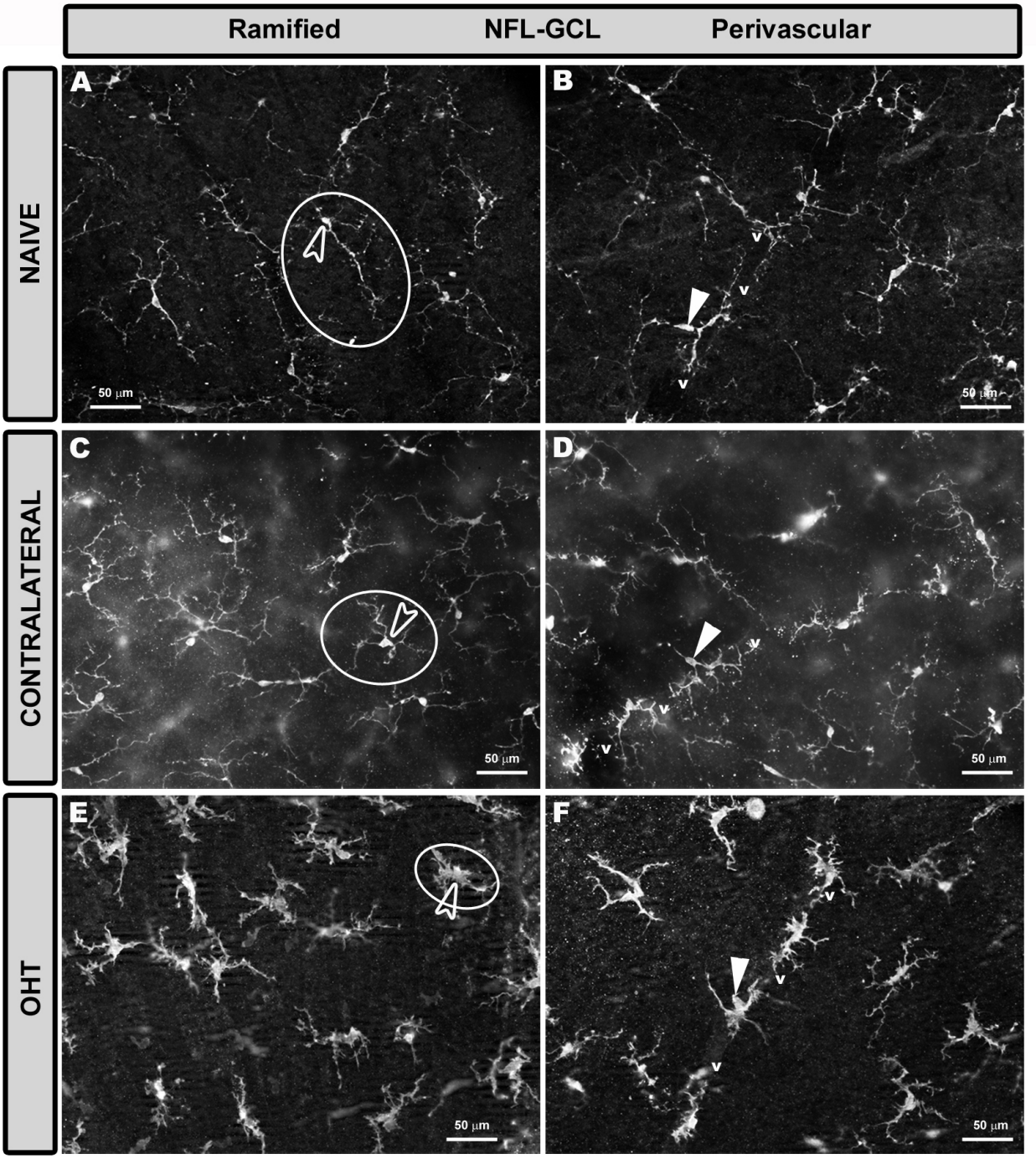
Ramified
NFL-GCL
Perivascular
NAIVE
CONTRALATERAL
OHT
A
B
C
D
E
F
50 μm

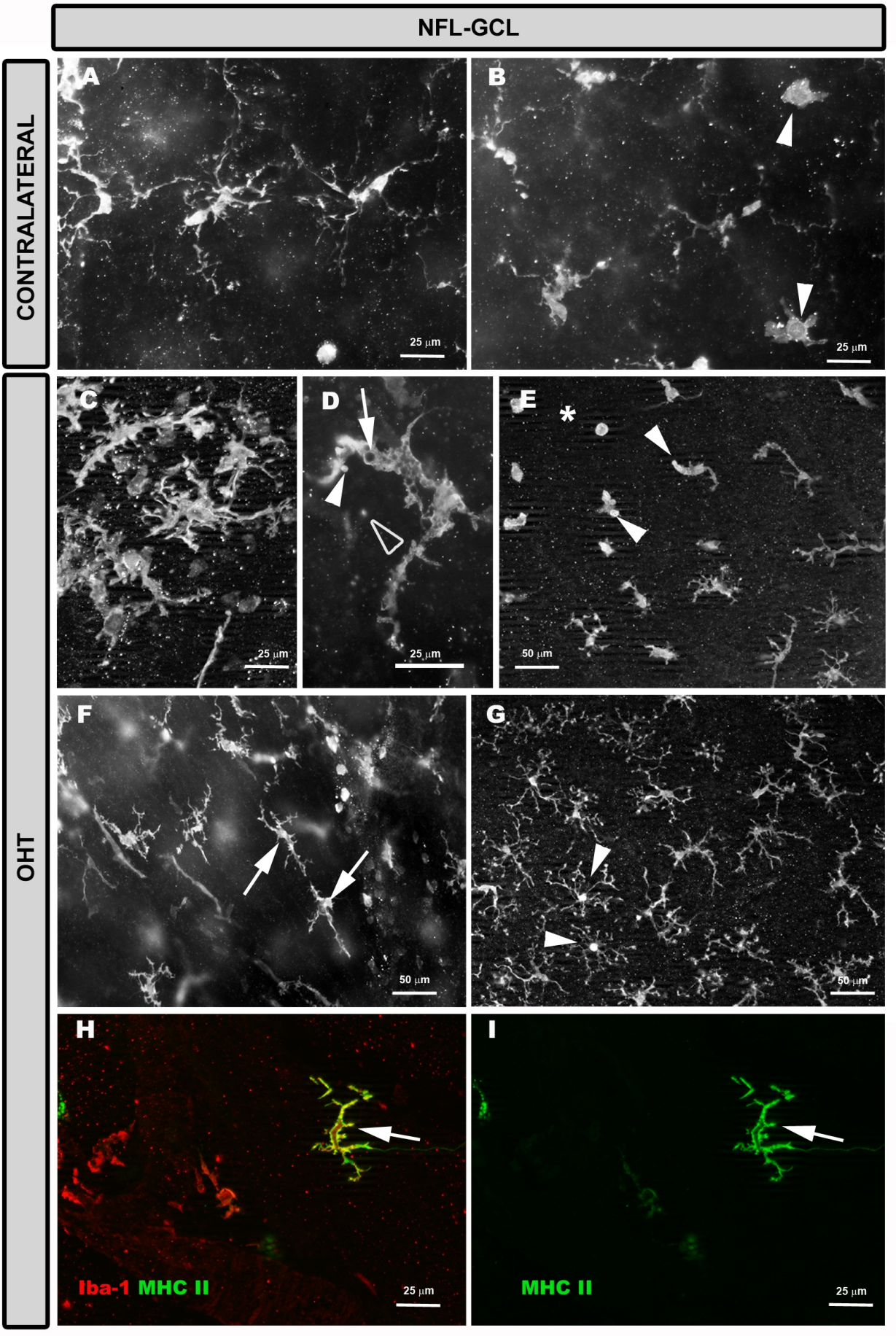
NFL-GCL
CONTRALATERAL
OHT
A
B
C
D
E
F
G
H
I
25 µm
25 µm
25 µm
25 µm
50 µm
50 µm
25 µm
Iba-1 MHC II
25 µm
MHC II
25 µm

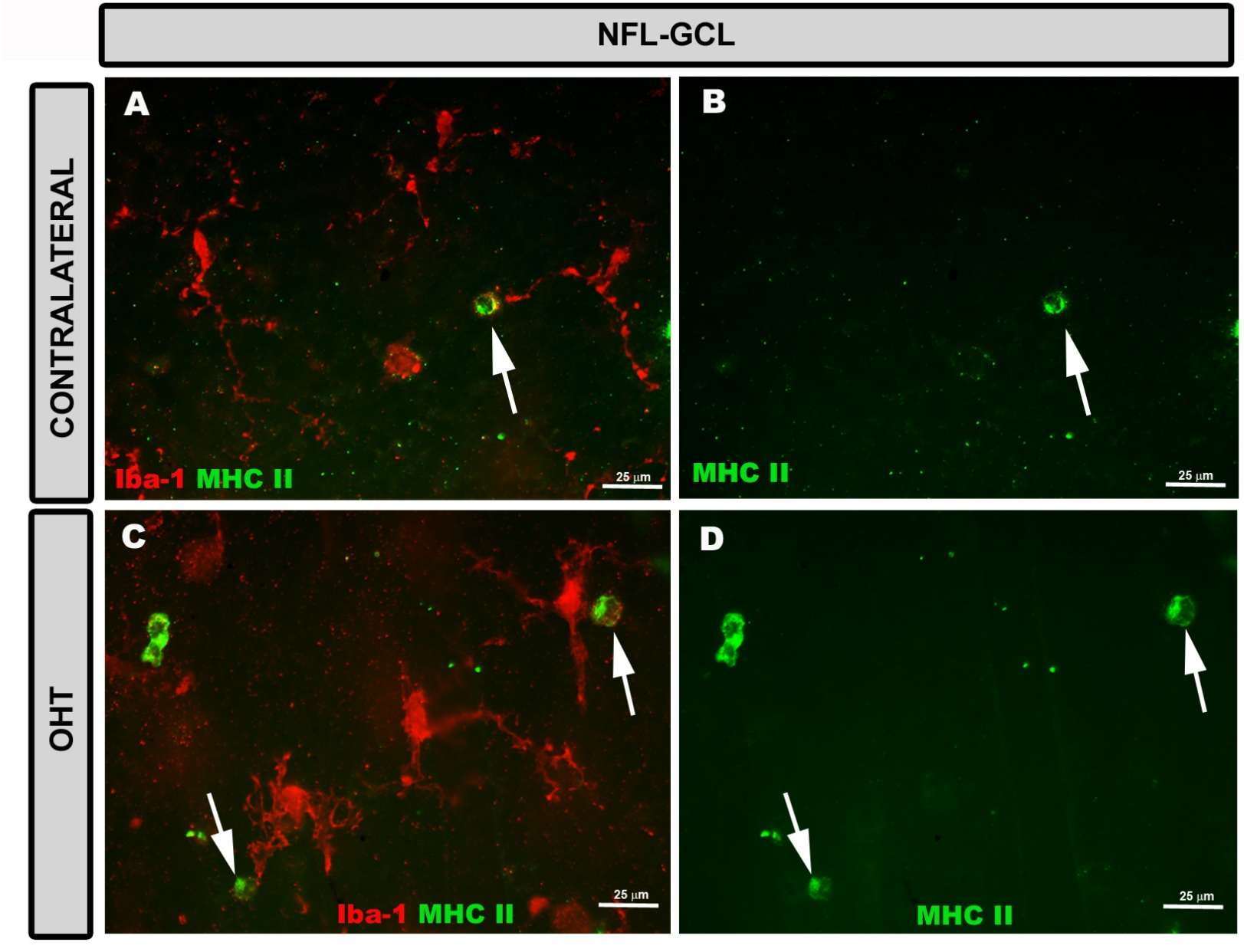
NFL-GCL
CONTRALATERAL
OHT
A
Iba-1 MHC II
25 µm
B
MHC II
25 µm
C
Iba-1 MHC II
25 µm
D
MHC II
25 µm

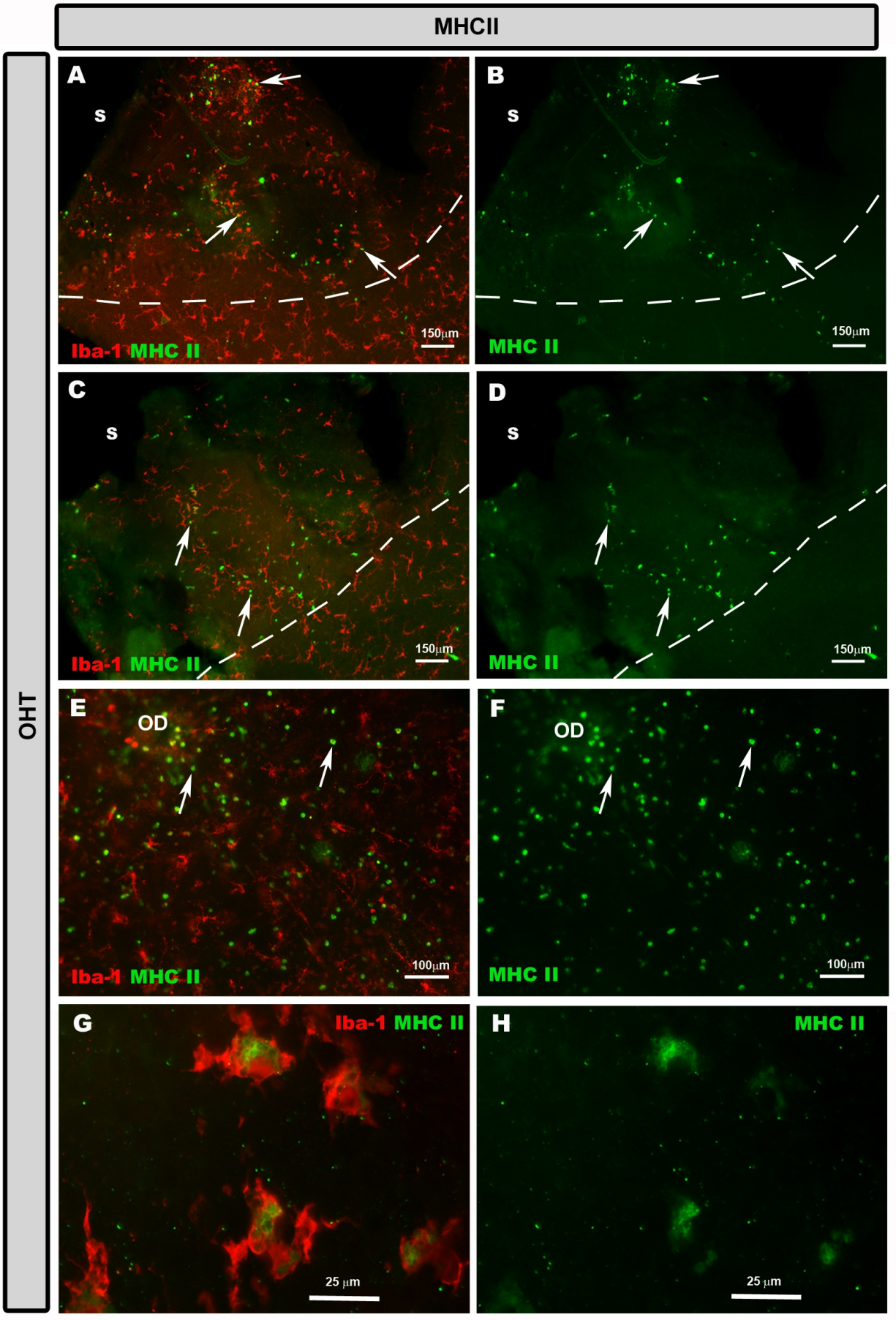
MHCII
OHT
A
S
Iba-1 MHC II
150μm
B
S
MHC II
150μm
C
S
Iba-1 MHC II
150μm
D
S
MHC II
150μm
E
OD
Iba-1 MHC II
100μm
F
OD
MHC II
100μm
G
Iba-1 MHC II
25 μm
H
MHC II
25 μm

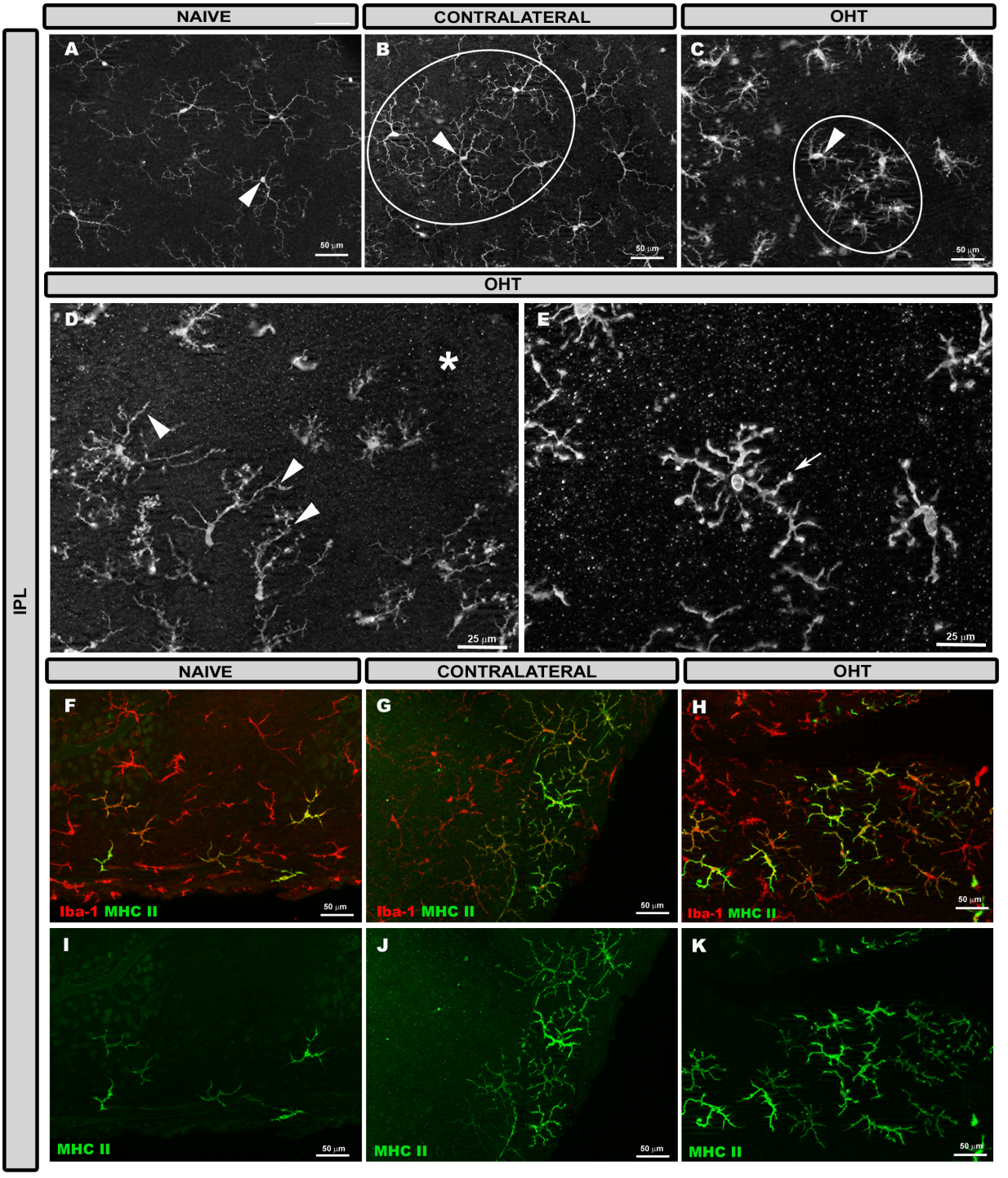
NAIVE
CONTRALATERAL
OHT
A
B
C
50 µm
OHT
D
E
*
25 µm
IPL
NAIVE
CONTRALATERAL
OHT
F
G
H
Iba-1 MHC II
I
J
K
MHC II

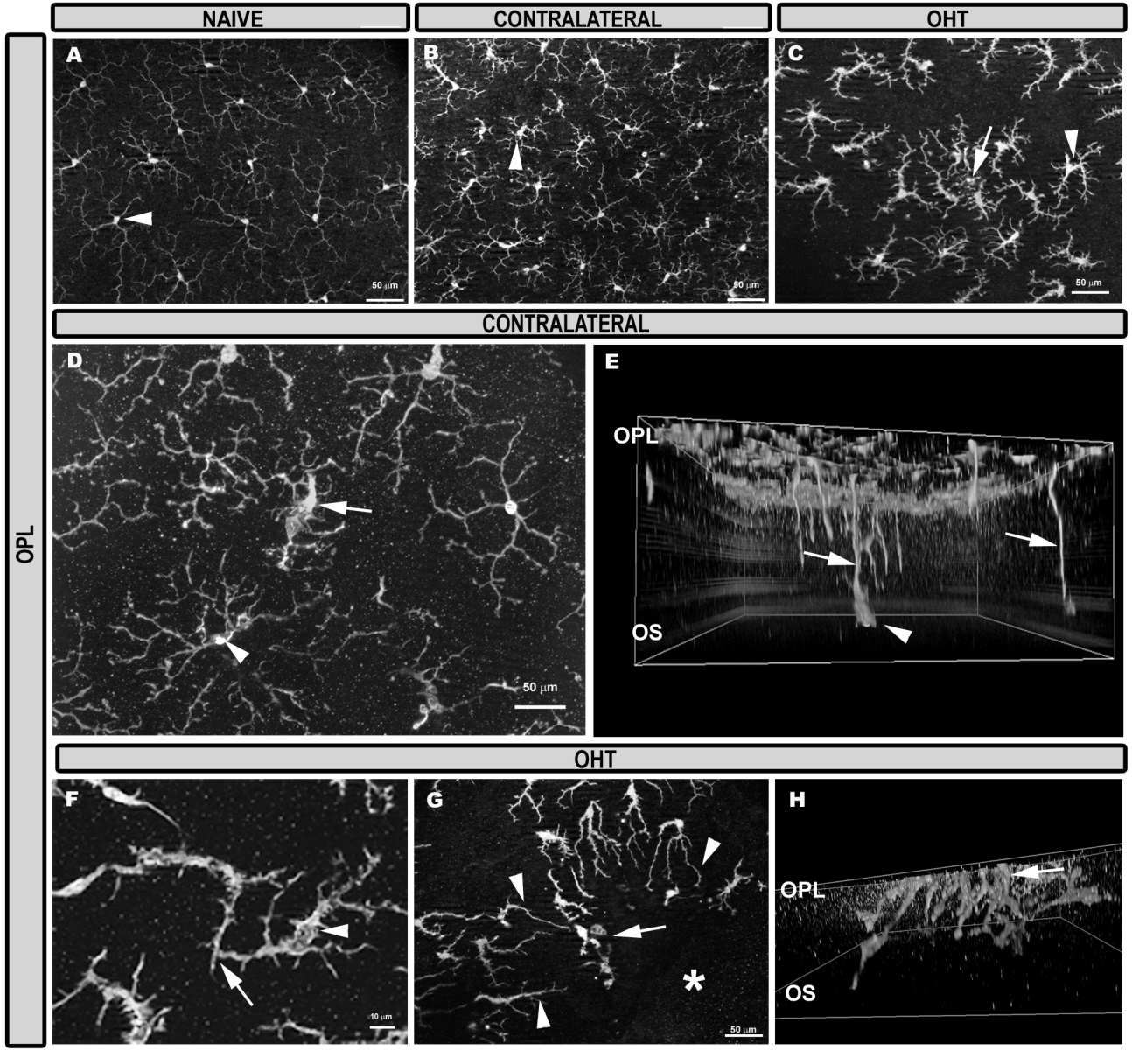
NAIVE
CONTRALATERAL
OHT
A
B
C
50 μm
50 μm
50 μm
CONTRALATERAL
D
E
OPL
OS
50 μm
OHT
F
G
H
OPL
OS
10 μm
50 μm
OPL

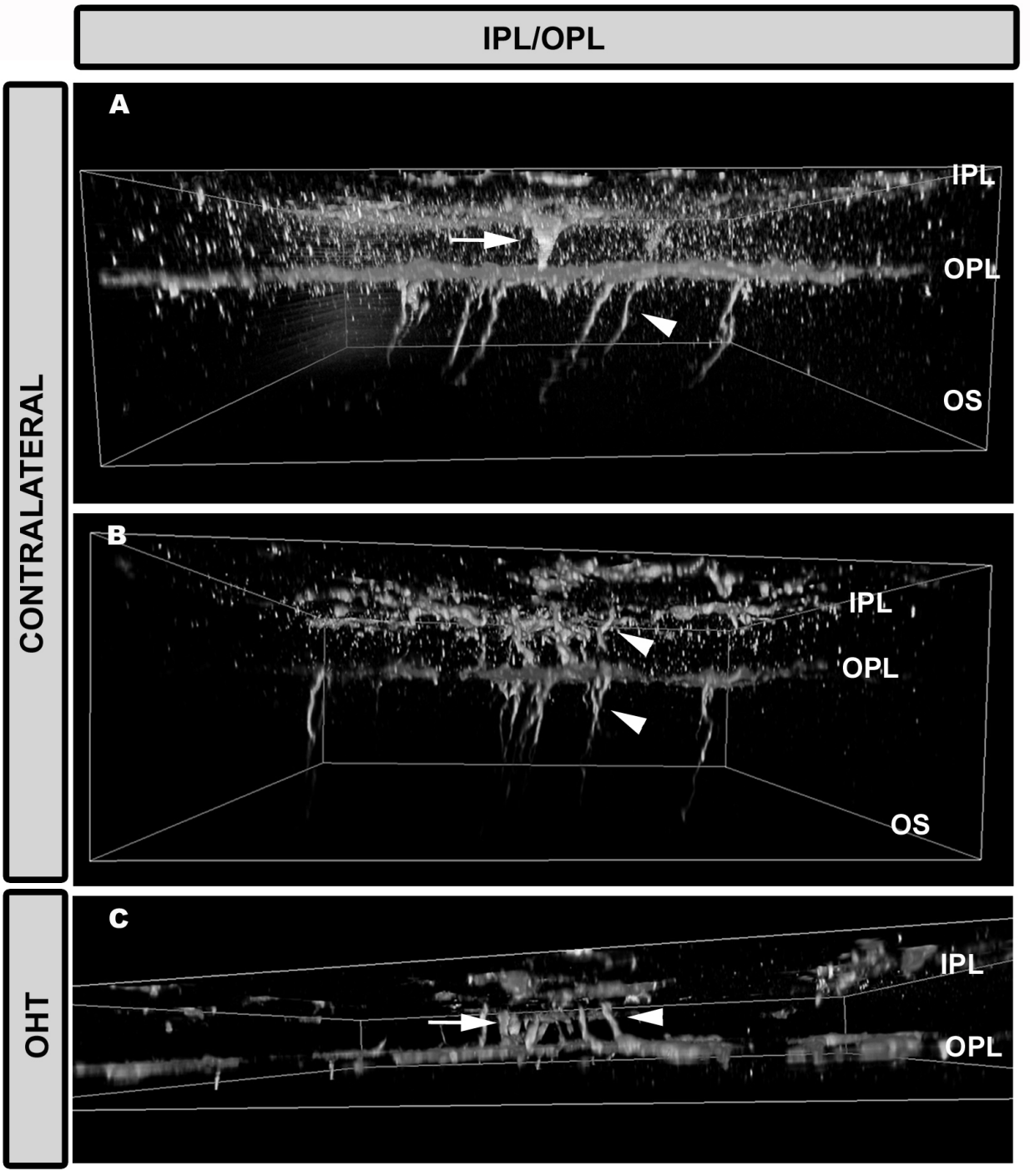
IPL/OPL
CONTRALATERAL
OHT
A
IPL
OPL
OS
B
IPL
OPL
OS
C
IPL
OPL

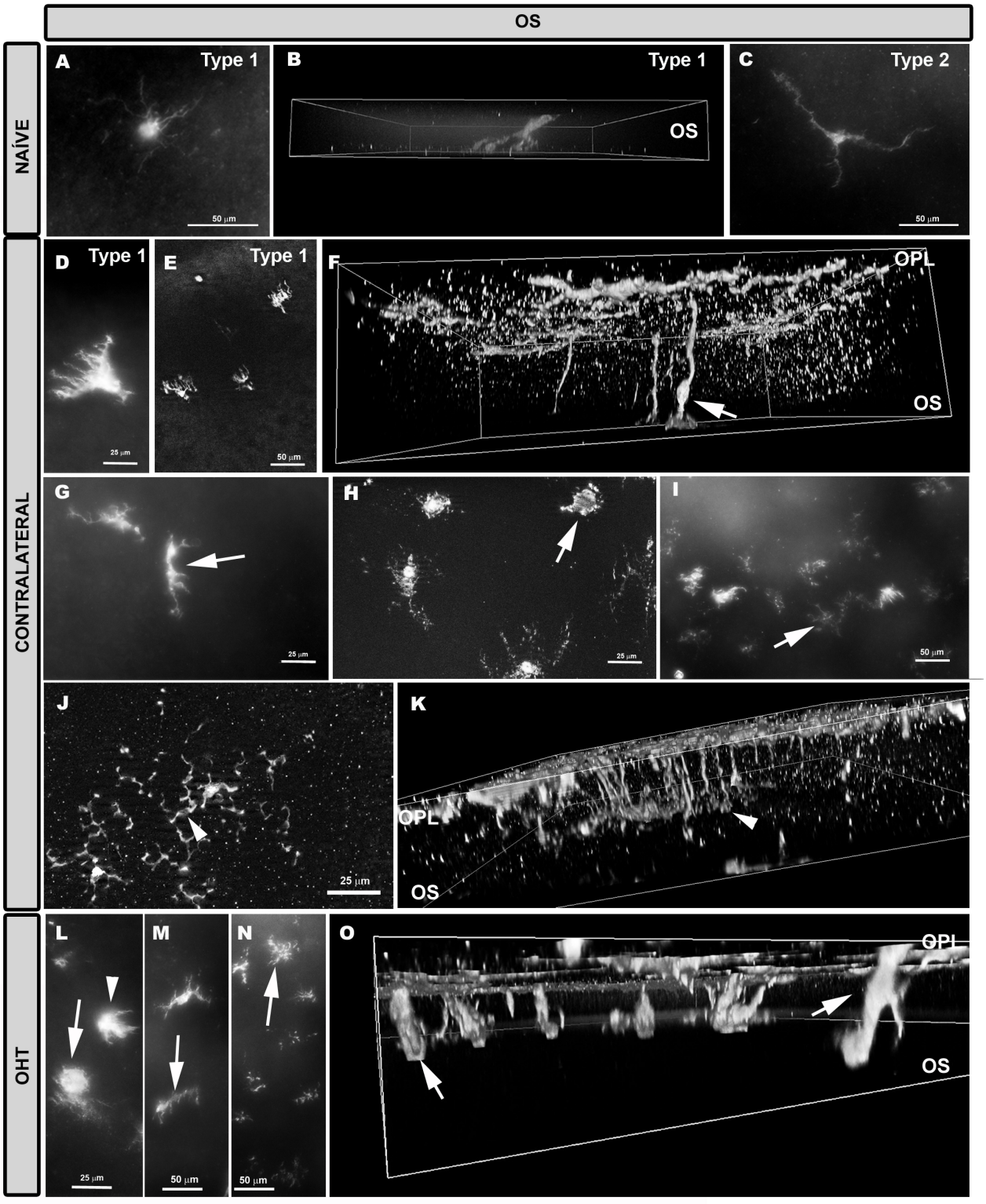
OS
NAÍVE
A
Type 1
50 μm
B
Type 1
OS
C
Type 2
50 μm
CONTRALATERAL
D
Type 1
25 μm
E
Type 1
50 μm
F
OPL
OS
G
25 μm
H
25 μm
I
50 μm
J
25 μm
K
OPL
OS
OHT
L
25 μm
M
50 μm
N
50 μm
O
OPL
OS

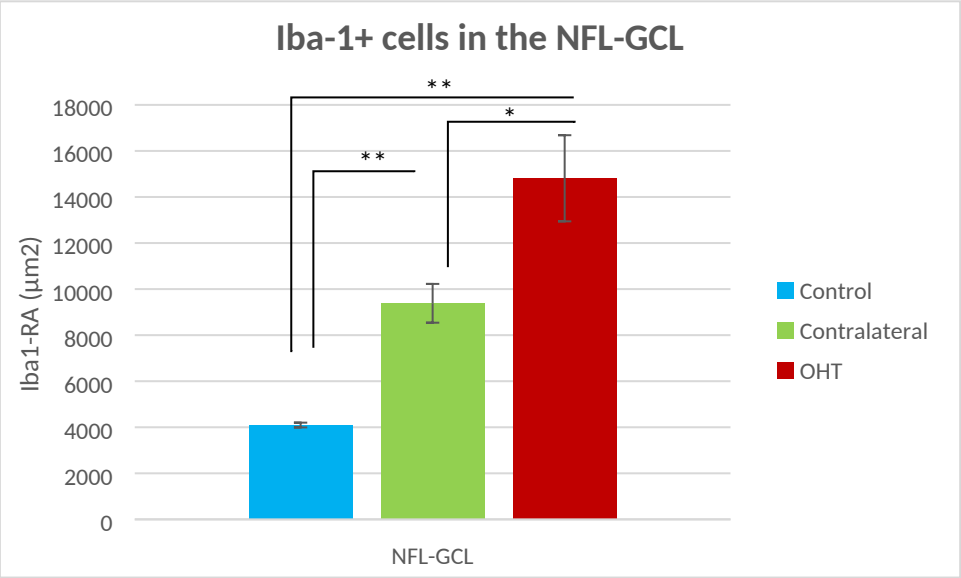
Iba-1+ cells in the NFL-GCL
Iba1-RA (µm2)
18000
16000
14000
12000
10000
8000
6000
4000
2000
0
**
**
*
NFL-GCL
Control
Contralateral
OHT

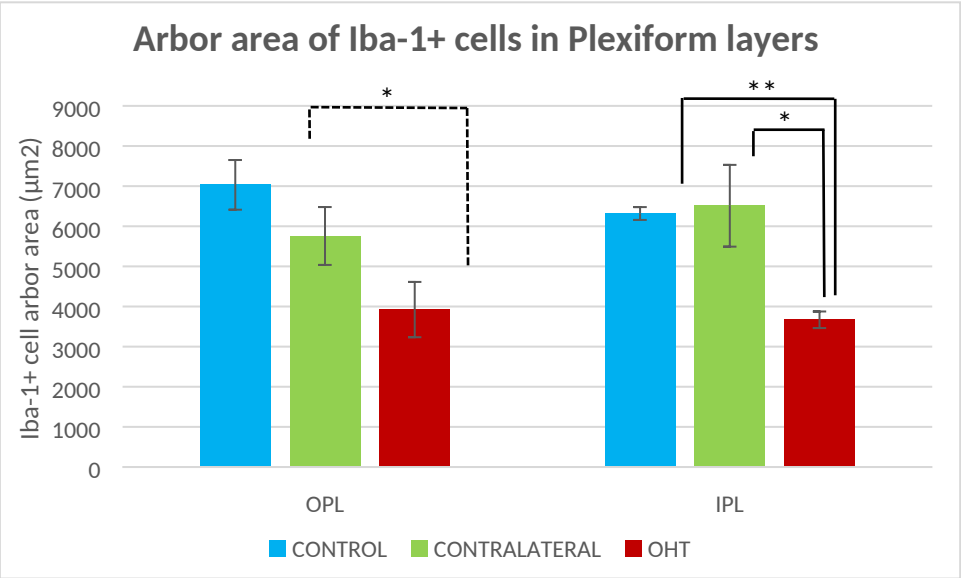
Arbor area of Iba-1+ cells in Plexiform layers
Iba-1+ cell arbor area (µm2)
9000
8000
7000
6000
5000
4000
3000
2000
1000
0
*
**
*
OPL
IPL
CONTROL
CONTRALATERAL
OHT

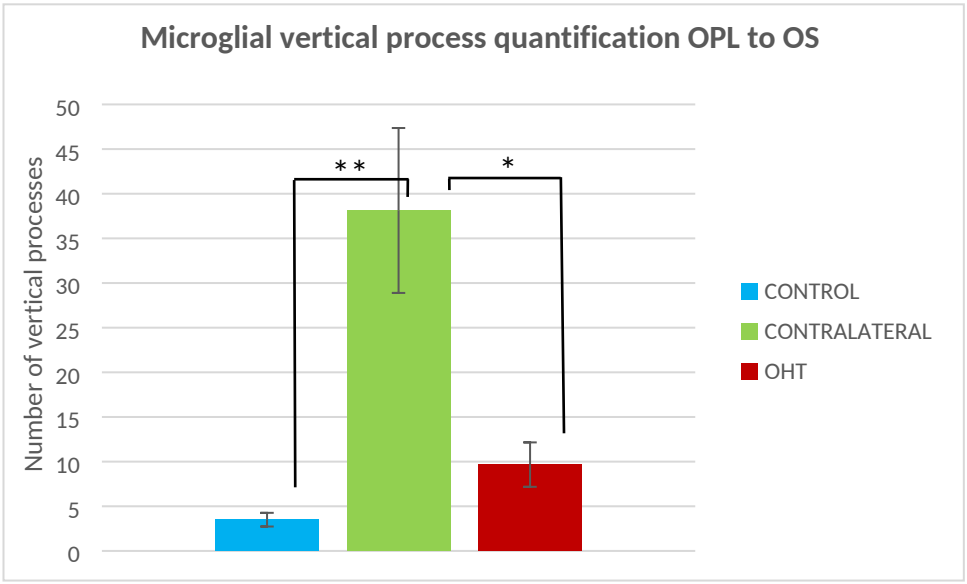
Microglial vertical process quantification OPL to OS
Number of vertical processes
50
45
40
35
30
25
20
15
10
5
0
* *
*
CONTROL
CONTRALATERAL
OHT

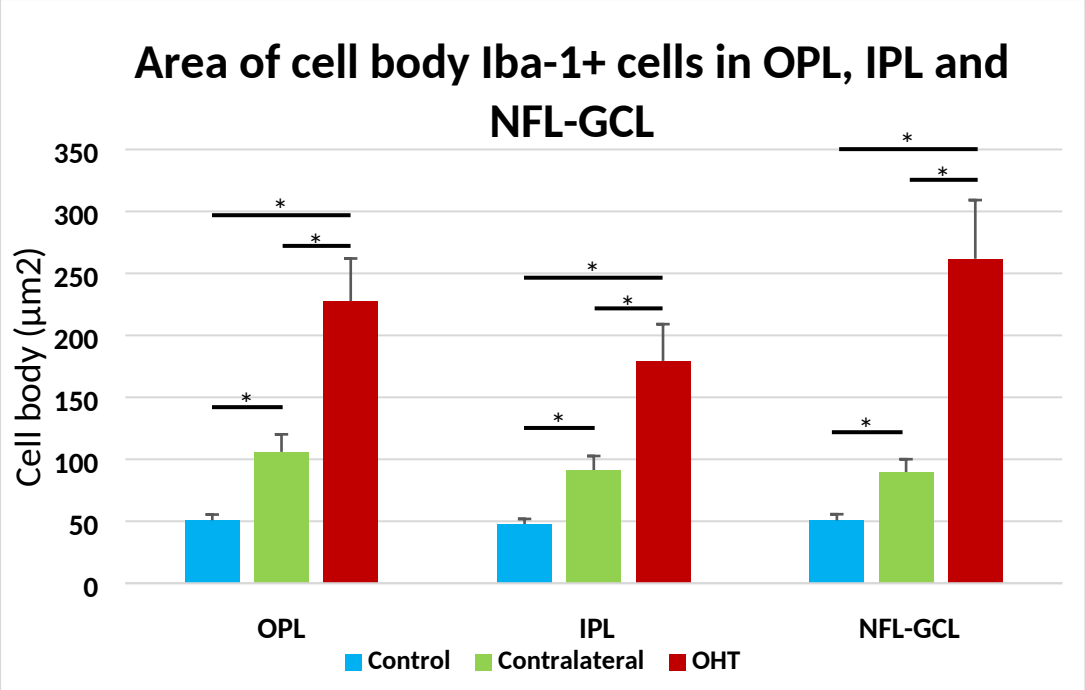
Area of cell body Iba-1+ cells in OPL, IPL and NFL-GCL
Cell body (µm2)
350
300
250
200
150
100
50
0
*
OPL
IPL
NFL-GCL
Control
Contralateral
OHT

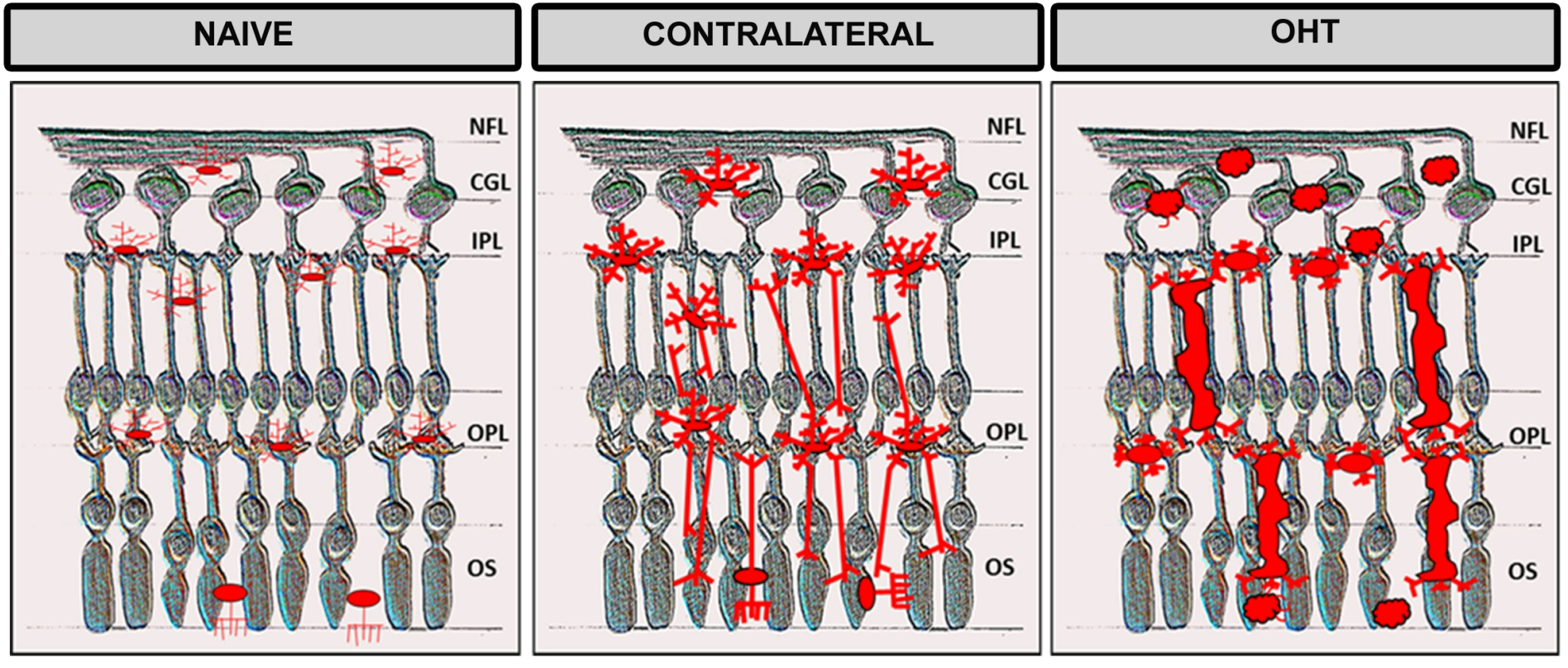
NAIVE
CONTRALATERAL
OHT
NFL
CGL
IPL
OPL
OS
NFL
CGL
IPL
OPL
OS
NFL
CGL
IPL
OPL
OS

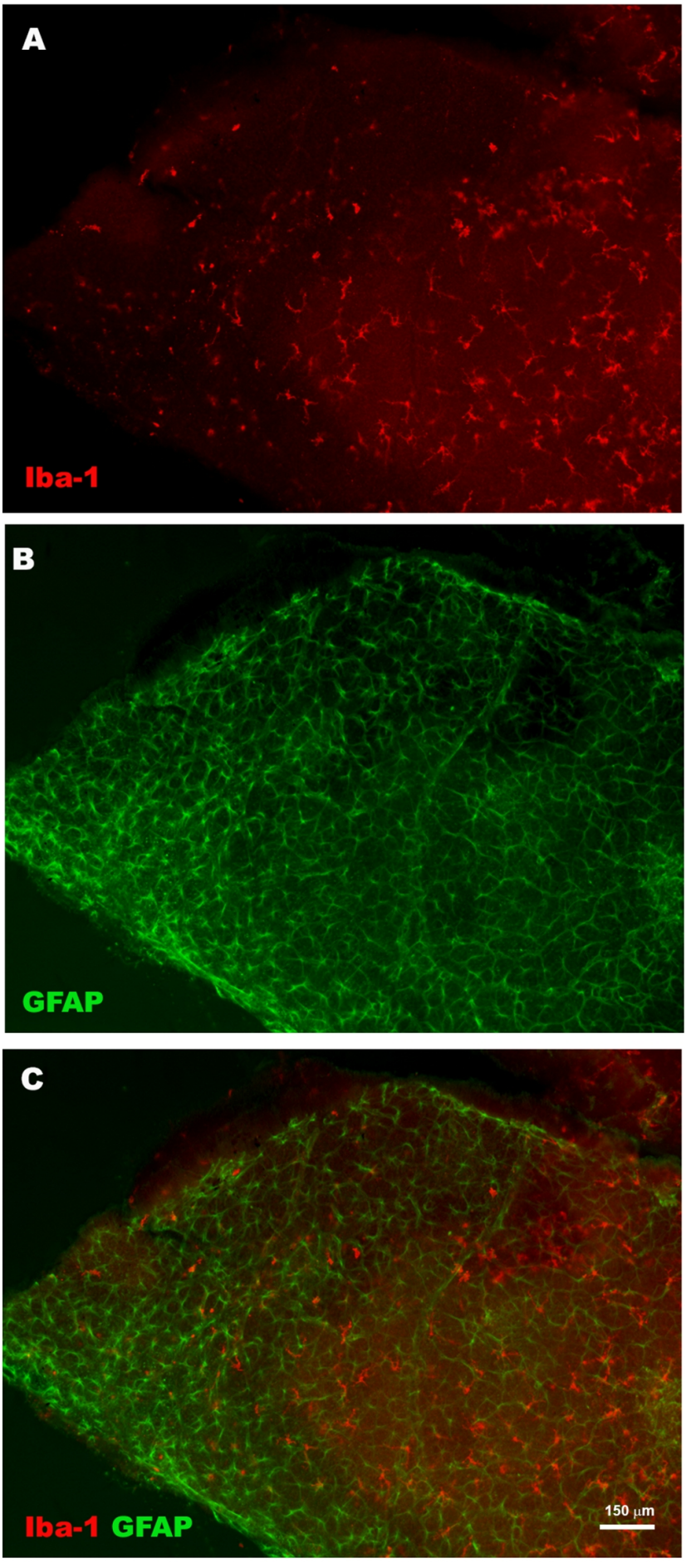
A
Iba-1
B
GFAP
C
Iba-1 GFAP
150 μm